Article

Lessons from (S)-6-(1-(6-(1-Methyl-1H-pyrazol-4-yl)-[1,2,4]triazolo[4,3-b]pyridazin-3-yl)ethyl)quinoline (PF-04254644), an Inhibitor of Receptor Tyrosine Kinase c-Met with High Protein Kinase Selectivity, but Broad Phosphodiesterase Family Inhibition Leading to Myocardial Degeneration in Rats

Jean Cui, Hong Shen, Michelle Tran-Dubé, Mitchell Nambu, Michele A McTigue, Neil Grodsky, Kevin Ryan, Shinji Yamazaki, Shirley Aguirre, Max Parker, Qiuhua Li, Helen Y Zou, and James G. Christensen

Just Accepted

Lessons from (*S*)-6-(1-(6-(1-Methyl-1*H*-pyrazol-4-yl)-[1,2,4]triazolo[4,3-*b*]pyridazin-3-yl)ethyl)quinoline (PF-04254644), an Inhibitor of Receptor Tyrosine Kinase c-Met with High Protein Kinase Selectivity, but Broad Phosphodiesterase Family Inhibition Leading to Myocardial Degeneration in Rats

J. Jean Cui, Hong Shen, Michelle Tran-Dubé, Mitchell Nambu, Michele McTigue, Neil Grodsky, Kevin Ryan, Shinji Yamazaki, Shirley Aguirre, Max Parker, Qiuhua Li, Helen Zou, and James Christensen*

La Jolla Laboratories, Pfizer Worldwide Research and Development, 10770 Science Center Drive, San Diego, CA 92121

ABSTRACT

The HGF/c-Met signaling axis is deregulated in many cancers and plays important roles in tumor invasive growth and metastasis. Exclusively selective c-Met inhibitor (*S*)-6-(1-(6-(1-methyl-1*H*-pyrazol-4-yl)-[1,2,4]triazolo[4,3-*b*]pyridazin-3-yl)ethyl)quinoline (**8**) was discovered from a highly selective HTS hit *via* structure based drug design and medicinal chemistry lead optimization. **8** had many attractive properties meriting preclinical evaluation. Broad off-target screens identified **8** as a pan-PDE family inhibitor which was implicated in a sustained increase in heart rate, increased cardiac output, and decreased contractility indices, as well as myocardial degeneration in *in vivo* safety evaluations in rats. **8** was terminated as a preclinical candidate because of a narrow therapeutic window in cardio-related safety. The learning from multi-parameter lead optimization and strategies to avoid the toxicity attrition at the late stage of drug discovery are discussed.

INTRODUCTION

c-Met, also called hepatocyte growth factor receptor (HGFR), belongs to a unique subfamily of receptor tyrosine kinases including macrophage stimulating 1 receptor RON. Hepatocyte growth factor (HGF), also known as scatter factor (SF), is the high-affinity natural ligand of c-Met. The HGF/c-Met signaling pathway plays important roles in invasive growth during embryo development and postnatal organ regeneration, and is only fully active in adults for wound healing and tissue regeneration processes.[1] However, the HGF/c-Met axis is frequently hijacked by cancer cells for tumorigenesis, invasive growth, and metastasis.[1,2] HGF and/or c-Met are expressed at abnormally high levels in a large variety of solid tumors including liver, breast, pancreas, lung, kidney, bladder, ovary, brain, prostate, gallbladder myeloma and many others, that are frequently associated with a metastatic phenotype and poor prognosis.[3] Various c-Met

mutations have been identified in many tumors, including hereditary and sporadic human papillary renal carcinomas, ovarian cancer, childhood hepatocellular carcinomas, gastric cancer, and lung cancer.[3] The activa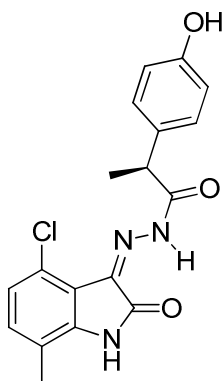tion of HGF/c-Met signaling plays important roles in resistance to EGFR and BRAF kinase inhibitors. *MET* amplification has been detected in up to 20% of NSCLC patients with EGFR mutations and who acquired resistance to gefitinib or erlotinib treatment.[4] Growth factor-driven resistance from tumor microenvironment represents another potential mechanism to anticancer kinase inhibitors.[5] HGF is present in melanoma patient's stromal cells and correlates with a poor response to the BRAF inhibitor vemurafenib treatment.[6] The upregulation of stromal HGF confers resistance to vemurafenib in BRAF-mutant melanoma cells.[6] Because of the role of aberrant HGF/c-Met signaling in human oncogenesis, invasion/metastasis, and resistance, the inhibition of this pathway has great potential in cancer therapy.[7] There are three approaches in modulating HGF/c-Met signaling currently in human clinical studies for oncology applications including the anti-HGF antibody (e. g. AMG 102, rilotumumab[8]), c-Met monoclonal antibody (e. g. MetMab[9]), and small molecule c-Met inhibitors (e. g. crizotinib[10], cabozantinib[11], and tivantinib[12]). Preliminary clinical benefits from the inhibition of HGF/c-Met signaling have been reported.[13] The c-Met monoclonal antibody MetMab in combination with erlotinib for non-small cell lung cancer significantly improved progression-free survival and overall survival, resulting in a near 3-fold reduction in the risk of death.[14] One patient with a *de novo* highly *MET*-amplified NSCLC achieved confirmed partial response with crizotinib.[15] While existing data have shown the potential of inhibiting the HGF/c-Met pathway, challenges remain in identifying specific patient populations as well as developing the right combination strategies (targeted agents, classic chemotherapy, or radiotherapy).[13]

Potent and specific kinase inhibitors are highly desired to validate the pharmacology of the proposed target and allow for effective combination with other agents for the maximum efficacy of cancer treatment. A highly specific c-Met HTS hit **1** (Chart 1) was discovered at legacy SUGEN/Pharmacia.[16] **1** was a highly selective, and ATP competitive c-Met inhibitor with high biochemical ligand efficiency (LE = -RTLogK_i/the number of heavy atoms = 0.42) and lipophilic efficiency (lipE = -LogK_i−cLogD = 4.80). Optimization of **1** by Koenig et al. afforded analogs with improved enzymatic and cellular potencies, as illustrated with compound **2** that has an enzymatic K_i of 1.3 nM and an IC_{50} of 7 nM for the inhibition of c-Met auto-phosphorylation in A549 cell line.[17] The cocrystal structure of **2** with unphosphorylated c-Met kinase domain (PDB ID 3zze) revealed an unexpected binding mode, having the phenol residue as a hinge binder and oxindole hydrazide interacting with the A-loop to stabilize the c-Met protein in an autoinhibitory inactive conformation.[16,18] Vojkovsky et al. designed the tetracyclic aromatic scaffold, exemplified by **3,** which proved to be an effective mimic of original oxindole hydrazide series.[19] The electron deficient tetracyclic ring retained the strong π-π stacking interaction with electron rich Tyr-1230, and could form hydrogen bonds with N-H of Asp-1226 and C=O of Arg-1208. Zhang et al. further chopped the non-druggable tetracyclic scaffold to the bicyclic triazolotriazine scaffold, exemplified by **4,** that revealed an even better ligand efficiency against c-Met than the tetracyclic scaffold despite the loss of the hydrogen bond with the carbonyl group of Arg-1208.[20] The electron deficiency of the bicyclic aromatic ring governs the strength of the interaction with Tyro-1230 at A-loop and is a determining factor for the potency and selectivity. Therefore, the triazolopyrazine scaffold, exemplified by **5**[21] and the triazolopyridazine scaffold, exemplified by **6,** are less potent in general.
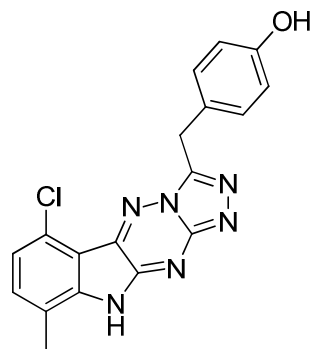
Chart 1. The discovery of highly selective c-Met inhibitors.
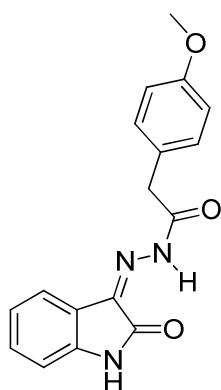
1
c-Met K_i 0.101 μM
c-Met cell IC_{50} >10 μM

2
c-Met K_i 0.0013 μM
c-Met cell IC_{50} 0.007 μM

3
c-Met K_i 0.0107 μM
c-Met cell IC_{50} 0.007 μM

4
c-Met K_i 0.0107 μM
c-Met cell IC_{50} 0.007 μM
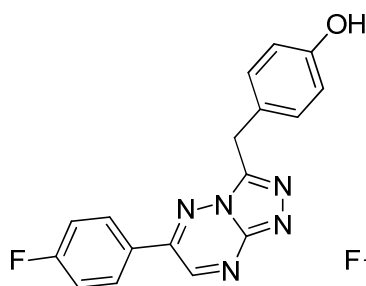
5
c-Met K_i 0.0198 μM
c-Met cell IC_{50} 0.141 μM

6
c-Met K_i 0.316 μM
c-Met cell IC_{50} 1.31 μM

The initial chemistry efforts on discovering the unique c-Met binding mode and the critical chemical scaffolds for exclusively selective and highly potent c-Met inhibitors (Chart 1) play an important role for the discovery and development of a class of exquisitely selective c-Met inhibitors into human clinical trials. The phenol hinge binder in the original chemistry series was successfully replaced with the conventional kinase hinge binder quinoline leading to **7** (Chart 2).[16] However, the triazolotriazine scaffold suffered with high non-P450 hepatocyte clearance.[16] Optimization of the less potent triazolopyrazine series produced the clinical compound **9** (PF-04217903).[16] The cocrystal structure of **9** with unphosphorylated c-Met kinase domain revealed the similar binding environment as **2,** and **9** was exquisitely selective over 208 kinases.[16] In

addition, the highly potent and selective c-Met inhibitors **10** (SGX-523)[22], **11** (JNJ-38877605)[23], **12** (INCB-28060)[24], and **13** (AMG-208)[25] were reported and have entered human clinical trials for potential oncology indications (Chart 2).

Chart 2. Exquisitely selective c-Met inhibitors.

7   **8**, PF-04254644   **9**, PF-04217903

10, SGX-523   **11**, JNJ38877605   **12**, INCB28060   **13**, AMG-208
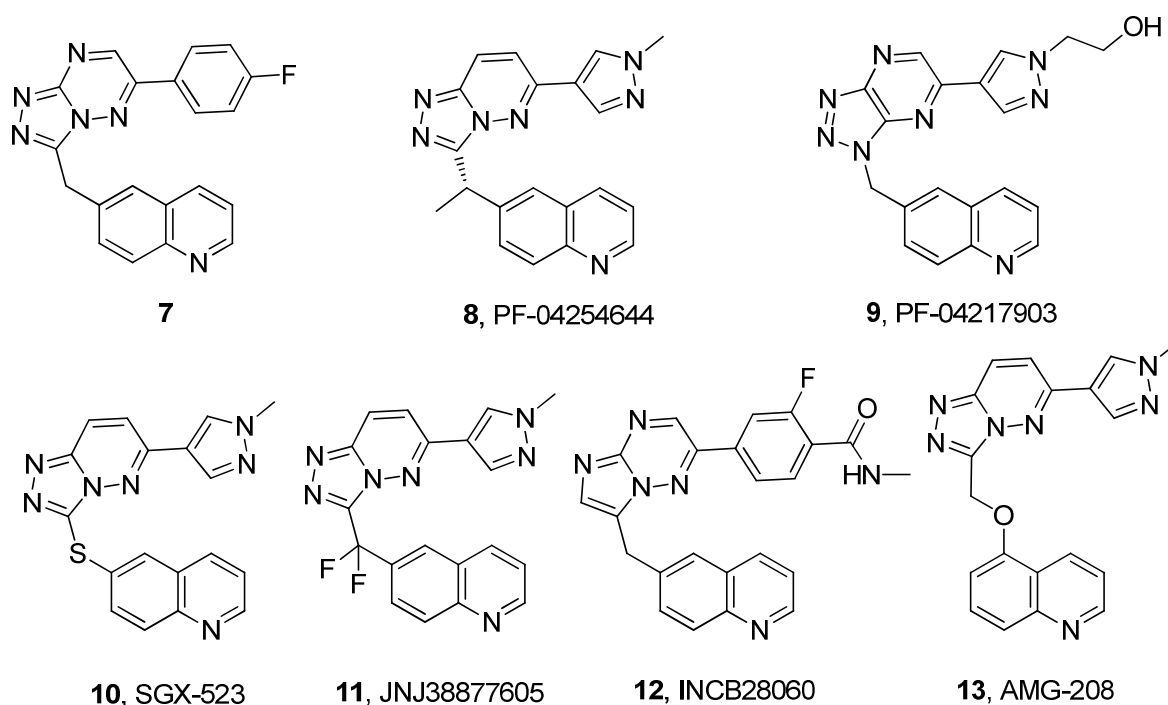
Herein, we report the medicinal chemistry lead optimization of the less potent triazolopyridazine series leading to the discovery of (*S*)-6-(1-(6-(1-methyl-1*H*-pyrazol-4-yl)-[1,2,4]triazolo[4,3-*b*]pyridazin-3-yl)ethyl)quinoline (**8**). The effort was conducted in parallel with the optimization of the triazolopyrazine series leading to the discovery of the clinical candidate **9**.[16] **8** and **9** were potent and exquisitely selective ATP competitive c-Met inhibitor, and demonstrated low nM potency against c-Met in both *in vitro* cell assays and *in vivo* target modulation studies. Both compounds showed effective tumor growth inhibition with good oral PK properties. However, **8** was also a potent phosphodiesterase family inhibitor, which proved to be responsible for a sustained increase in heart rate, increased cardiac output, and decreased

contractility indices, as well as myocardial degeneration in rats. **8** was terminated as a preclinical candidate because of a narrow therapeutic window in cardio-related safety. **9**, which has a higher LipE value for c-Met than **8,** has a clean kinase selectivity profile, and also has a cleaner profile in a broad off-target screen. This favorable profile supported a large therapeutic window in *in vivo* animal tolerance studies. **9** was selected as preclinical candidate and entered human clinical evaluations for cancer treatment.

Toxicity and serious adverse events in late stage drug development are the major causes of drug failure. The adverse toxicologic effects are further classified as on-target, and off-target effects. The on-target toxicity reflects the exaggerated and adverse pharmacologic effects of the interested target which may lead to the termination of a drug development based on the target. The off-target adverse effects are a result of modulation of biologically unrelated targets which should be avoided at the early drug discovery stage. Although kinase selectivity has been a major challenge in kinase drug development because of the conservation of the ATP binding pocket among kinases, the off-targets outside the protein kinase family deserve equal attentions at the early drug discovery stage. Both **8** and **9** are highly selective c-Met RTK inhibitors. However, the off-target effects from the inhibition of PDE family leading to a narrow therapeutic window in cardio-related safety result in the terminate of **8** as a preclinical candidate. The learning from multi-parameter lead optimization and strategies to avoid the late stage toxicity attrition will be discussed here.

RESULTS AND DISCUSSION

The triazolotriazine chemical series, represented with **7** (Chart 2), was successfully designed as a class of potent and kinase-selective c-Met inhibitors evolving from the HTS hit **1**.[16] The quinoline group functions as a hinge binder and the triazolotriazine group plays an important role

in both c-Met cellular potency and kinase selectivity *via* the unique interaction with the A-loop residue Tyr-1230 (Figure 1).   The unique autoinhibitory position of the A-loop in unphosphorylated c-Met has been documented in c-Met crystal structures, including apo-c-Met.[26] In particular, many c-Met inhibitors form interactions with Tyr-1230, and the interactions vary in strength and contribute to different affinities and selectivity.[16]   Although it had an attractive potency and selectivity profile, the triazolotriazine series suffered high clearance in human hepatocyte, and was de-prioritized.[16] Alternatively, the less potent triazolopyrazine (represented with **5**) and triazolopyridazine (represented with **6**) series were explored.   The detailed medicinal chemistry lead optimization of the triazolopyrazine series leading to the clinic candidate **9** was reported previously[16], and some of the data are cited here as direct comparisons with the triazolopyridazine series for illustration of the learning.   We previously reported the selection of quinoline as a suitable hinge binder with good potency and metabolic stability in the triazolopyrazine series in the replacement of phenol hinge binder in **1**.[16]   Here, the quinoline group was directly used as the desired hinge binder in the triazolopyridazine series for the further lead optimization at the 6-position.   With the replacement of N-7 in the triazolotriazine core with a carbon atom, the triazolopyridazine bicyclic aromatic ring is more electron rich, resulting in a less effective interaction with Tyr-1230.   As a result, weaker potencies were generally observed in the triazolopyridazine series (**A**-series) as demonstrated with **14A**.   **14A** was about 10-fold less potent in both enzymatic and cellular assays relative to **7.**   The structure activity relationship at the 6-position of the [1,2,4]triazolo[4,3-*b*]pyridazin-3-ylmethyl-quinoline series was investigated (Table 1) for the potential improvement of potency and ADME properties.   Overall, 6-substituted [1,2,4]triazolo[4,3-*b*]pyridazin-3-ylmethyl-quinolines were metabolically stable and had good permeability.   However, a flat SAR in potency was observed for 6-aryl compounds **14A−16A**

and **8A**. In general, the **A**-series was about 10-fold less potent than the **B**-series (the **B**-series was reported previously[16] and cited here for the comparison), as demonstrated with **8A** and **8B**. The electron donating amino and dimethylamino groups in **17A** and **18A** provided even weaker potencies. Consistently, **17A** was much less potent than the triazolopyrazine analogue **17B**.
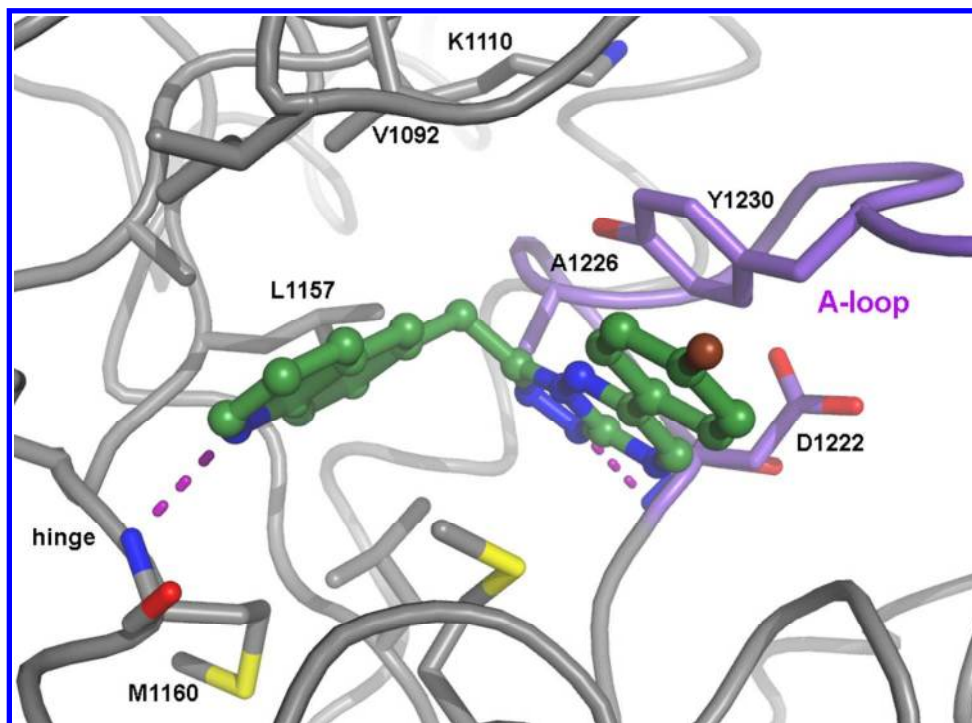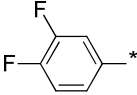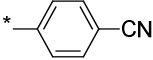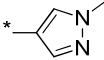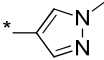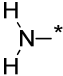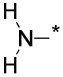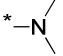
Figure 1. Cocrystal structure of **7** with the unphosphorylated c-Met kinase domain (PDB 3zbx).

Table 1. Structure activity relationship of 6-substituted [1,2,4]triazolo[4,3-*b*]pyridazin-3-ylmethyl-quinolines.
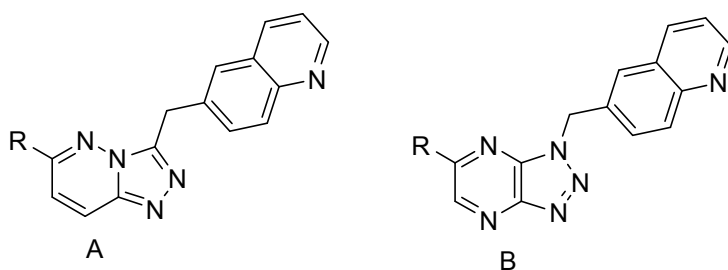
Compd	R	cLogD[a]	c-Met K_i	c-Met	LipE	HLM	Solub.

		$(\mu M)^b$	Cell IC$_{50}$ $(\mu M)^b$	$(IC_{50})^c$	CL$_{int, app}^d$	$(\mu M)^e$
7[22]		2.03	0.006	0.005	6.27	63.1	ND
14A		3.44	0.044	0.048	2.88	13.4	11.5
15A		3.65	0.013	0.019	4.07	22.7	19.1
16A		2.90	0.024	0.044	4.46	ND	ND
8A		1.73	0.074	0.044	5.63	ND	ND
8B		0.68	0.006	0.001	8.32	5.95	37.8
9		0.05	0.005	0.004	8.35	<7.6	22.2
17A		0.54	0.379	2.5	5.06	<7.6	453
17B		-0.95	0.015	0.034	8.42	<7.6	ND
18A		1.93	0.25	0.349	4.53	35	134

^{a} Calculated logarithm of the octanol/water distribution coefficient at pH 7.4 using ACD pchbat version 9.3. ^{b} Inhibition constants (K_i) and cell IC$_{50}$ were determined as described under Experimental Section. The coefficients of variance were typically less than 20% (n = 2). A549 human lung carcinoma cell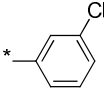 line was used for the evaluation of the inhibition of autophosphorylation of c-Met. ^{c} LipE (IC$_{50}$) = pIC$_{50}$ – cLogD. ^{d} Human liver microsomal intrinsic clearance (μL/min/mg). ^{e} Kinetic solubility at pH 6.5. ND, not determined.

The triazolopyridazine series has a cLogD value more than one log unit higher than the triazolopyrazine series, and coupled with the weaker inhibition, this leads to lipE values more than three log units lower than the triazolopyrazine series. Considering LipE, there is little advantage to continue working on the triazolopyridazine series. However, comprehensive analyses of the ADME properties of both series indicated that the triazolopyridazine series has much higher intrinsic human liver microsome metabolic stability relative to the triazolopyrazine series (Figure 2, log scale of human liver microsomal intrinsic clearance HLM $CL_{int.,app}$ vs cLogD). Overall, triazolopyridazines (blue square) were more metabolically stable than triazolopyrazines (red square) at higher cLogD value. Therefore, the triazolopyridazines could potentially provide a better chemistry space for multi-parameter optimizations on metabolic stability, permeability, and potency.
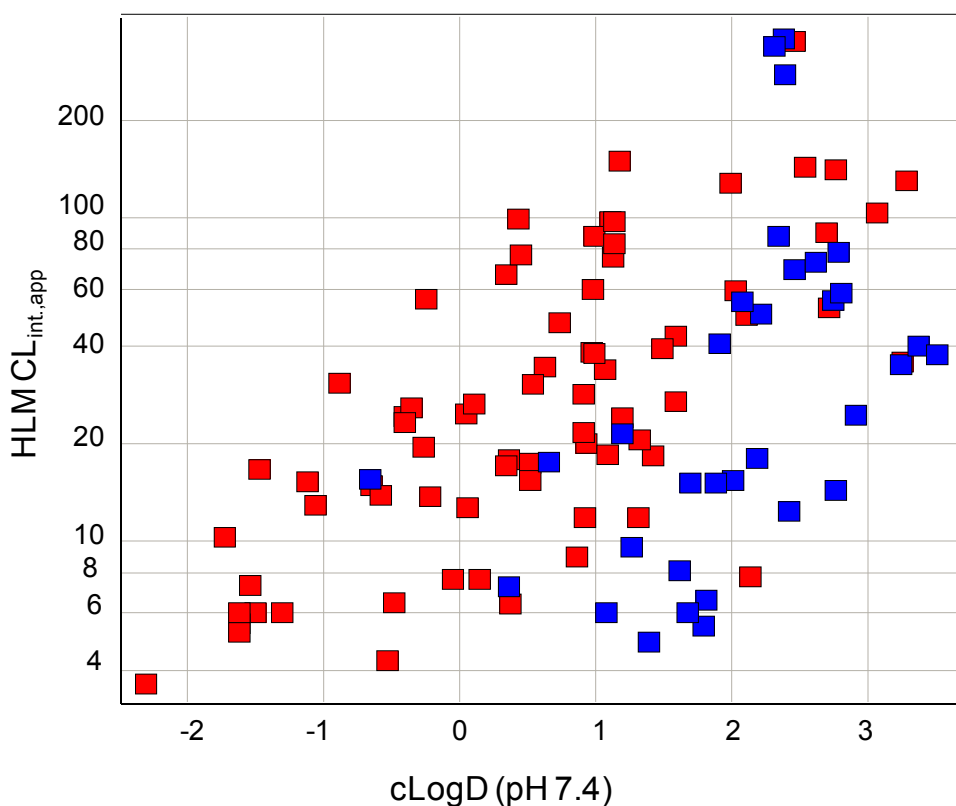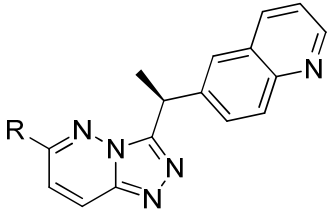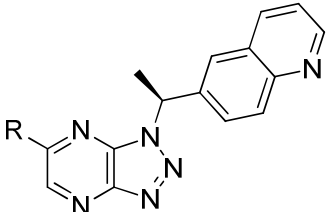
Figure 2. Metabolic clearance in human liver microsomes vs cLogD (red color for the triazolopyrazine series, and blue color for the triazolopyridazine series).

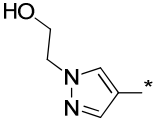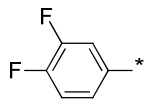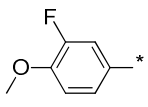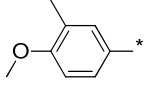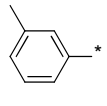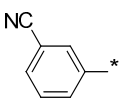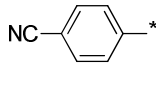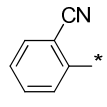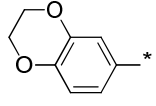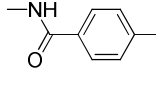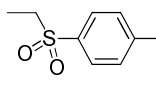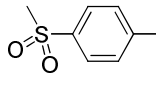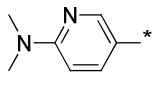Because of the attractive ADME properties, the triazolopyridazine series was explored further to improve the c-Met potency. The cocrystal structure of **7** with the unphosphorylated c-Met kinase domain revealed a small hydrophobic pocket for the potential improvement of the c-Met potency (Figure 1). The hinge binding quinoline substituent was linked with the triazolotriazine group *via* a methylene linker. The methylene group was adjacent to a hydrophobic pocket surrounding with the side hydrophobic chains of Lys-1110, Val-1092, Leu-1157 and Ala-1226. The modeling indicated that an (*S*)-methyl group could fit into the pocket well and potentially boost the potency. A series of compounds with an alpha-methyl group having the *S*-configuration were synthesized, and screened for the potency against c-Met (Table 2).
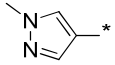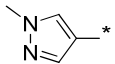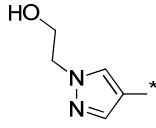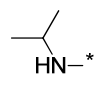
Indeed, the (*S*)-methyl group improved potency significantly as demonstrated with **14A** and **14C** (10-fold improvement for the enzymatic activity and 4-fold for the cellular potency). Although the introduction of a methyl group increased the lipophilicity (cLogD) by 0.35 unit, the dramatic improvement on potency caused the cell LipE of **14C** to increase by 1.25 unit relative to **14A**, which justified the introduction of a hydrophobic group, and also implied that the methyl group had a strong van der Waals interaction with the protein as originally designed. A broad set of R groups were investigated at the 6-position in **C**-series and **D**-series (Table 2) in order to identify the potential candidates with comprehensively acceptable properties. Overall, 6-aryl substituents provided good potency against c-Met. The substituents at *ortho*, *meta*, and *para*-positions of 6-phenyl group were well tolerated as demonstrated with compounds **14C−26C**. The R group in both the **C**- and **D**-series extended into the solvent-exposed area, and as expected, the substituents of both polar and hydrophobic groups didn't change the potency

significantly, however, the LipE and metabolic stability varied significantly according to the nature of the R groups. The *N* or *O*-alkyl substituents on 6-aryl group are highly cleared in human liver microsomes as demonstrated with compounds **19C**, **20C**, **23C** and **27C**. **21C** with a methyl group also showed a high metabolic clearance. The polar substituents including cyano group in **15C**, **16C**, and **22C**, amide group in **24C**, and sulfonyl group in **25C** and **26C** made the compounds potent and metabolically stable. In general, the 6-phenyl compounds in **C**-series had low solubility. **8** with *N*-methyl pyrazol-4-yl group had a lower cLogD of 2.07, and comparable potency in comparison with 6-phenyl compounds, which led to a much improved LipE (6.15), good metabolic stability and solubility. Consistently, the **D**-series was about 10 fold more potent than the **C**-series as shown with **8** and **8D**. Again, the (*S*)-methyl group improved the potency of 6-*N*-substituted compounds as exemplified by **28C**, which demonstrated an overall good profile, especially in solubility (433 μM). The contribution of the magic (*S*)-methyl group to the potency was further observed with the direct comparison of **9** and **9D**. Although the **D**-series was much more potent, the **C**-series had better solubility as illustrated with **8** (60.4 μM) and **8D** (16.3 μM).

Table 2. Structure activity relationship of 6-substituted (*S*)-6-(1-[1,2,4]triazolo[4,3-*b*]pyridazin-3-yl)ethyl)quinolines and (*S*)-6-(1-1*H*-[1,2,3]triazolo[4,5-*b*]pyrazin-1-yl)ethyl)quinolines.

Compd	R	cLogD[a]	c-Met K_i (μM)[b]	c-Met Cell IC_{50} (μM)[b]	LipE (IC_{50})[c]	HLM $CL_{int, app}$[d]	Solub. (μM)[e]

14C		3.79	0.004	0.012	4.13	13.4	8.73
19C		3.71	0.004	0.008	4.39	281	10.9
20C		4.2	0.003	0.009	3.85	304	1.77
21C		4.39	0.005	0.011	3.57	81.8	19.0
15C		4.0	0.004	0.004	4.40	17.9	32.5
16C		3.24	0.008	0.012	4.68	12.1	15.5
22C		3.18	0.006	0.005	5.12	23.1	213
23C		3.34	0.004	0.006	4.88	304	6.08
24C		2.46	0.007	0.015	5.36	12.2	11.0
25C		2.63	0.024	0.036	4.81	10.4	136
26C		2.1	0.012	0.024	5.52	<7.6	44.9
27C		3.29	0.008	0.025	4.31	232	16.2

		$LogD^a$	K_i^b	IC_{50}^b	$LipE^c$	Cl_{int}^d	Sol^e
8		2.07	0.0103	0.006	6.15	<7.60	60.4
8D		1.02	0.0014	0.0007	8.13	<7.6	16.3
9D		0.40	0.0028	0.0005	8.90	<7.6	17.3
28C		2.42	0.007	0.023	5.22	20.2	433

[a] Calculated logarithm of the octanol/water distribution coefficient at pH 7.4 using ACD pchbat version 9.3. [b] Inhibition constants (K_i) and cell IC_{50} were determined as described under Experimental Section. The coefficients of variance were typically less than 20% (n = 2). A549 human lung carcinoma cell line was used for the evaluation of the inhibition of autophosphorylation of c-Met. [c] LipE (IC_{50}) = pIC_{50} − cLogD. [d] Human liver microsomal intrinsic clearance (μL/min/mg). [e] Kinetic solubility at pH 6.5.

To test whether the effect of the alpha-methyl group is universal for the different hinge binders, a subseries with azaindole hinge binder was investigated (Table 3). As a direct comparison, **8F** with (*S*)-methyl group was 10 fold more potent than **8E**. **8F−29F** with the azaindole hinge binder had a similar potency as the analogues in **C**-series having the quinoline hinge binder, however, **8F−29F** provided better solubility profiles. The metabolite identification study of **8F** indicated the presence of the GSH-adducts at azaindole and methylene positions (Figure S1), and the **F**-series was de-prioritized.

Table 3. Structure activity relationship of 6-substituted 3-(1-(1*H*-pyrrolo[2,3-*b*]pyridin-3-yl)ethyl)-[1,2,4]triazolo[4,3-*b*]pyridazines

E

F

Compd	R	cLogD[a]	c-Met K$_i$ (μM)[b]	c-Met Cell IC$_{50}$ (μM)[b]	LipE (IC$_{50}$)[c]	HLM CL$_{int, app}$[d]	Solub. (μM)[e]
8E	*—pyrazole(N–)	1.46	0.0897	0.209	5.22	<7.6	111
8F	*—pyrazole(N–)	1.81	0.016	0.0176	5.94	<7.6	150
16F	*—C$_6$H$_4$—CN	2.98	0.0149	0.023	4.66	28	ND
28F	*—NH—CH(CH$_3$)$_2$	2.16	0.0101	0.019	5.56	25	475
29F	*—NH—cyclopropyl	1.81	0.0167	0.0254	5.78	18	426

[a] Calculated logarithm of the octanol/water distribution coefficient at pH 7.4 using ACD pchbat version 9.3. [b] Inhibition constants (K$_i$) and cell IC$_{50}$ were determined as described under Experimental Section. The coefficients of variance were typically less than 20% (n = 2). A549 human lung carcinoma cell line was used for the evaluation of the inhibition of autophosphorylation of c-Met. [c] LipE (IC$_{50}$) = pIC$_{50}$ − cLogD. [d] Human liver microsomal intrinsic clearance (μL/min/mg). [e] Kinetic solubility at pH 6.5. ND, not determined.

Collectively, a number of compounds achieved good potency and *in vitro* ADME profiles, and were selected for *in vivo* rat PK studies (Table 4) and *in vitro* toxicity evaluations. The rat *in vivo* PK data of **9** was cited as a reference for the comparison.[16] **8**, **14C** and **15C** demonstrated moderate plasma clearance and volume distribution. **8** and **14C** showed good oral bioavailability, and **14C** and **15C** have good half life.

Table 4. *in vivo* Rat pharmacokinetic properties.

Compd	MW	pK_a[a]	$cLogD$[b]	$eLogD$[c]	CL_{plasma} (mL/min/kg)	V_{ss} (L/kg)	$T_{1/2}$ (h)	F_{oral} %	c-Met Cell $eLipE$[d]
9	372	4.66	1.68	1.38	8.2	1.6	3.7	71	7.02
8	355	4.79	2.07	2.05	21	3.5	1.9	58	6.17
14C	387	4.79	3.79	3.07	31	3.6	3.6	52	4.75
15C	376	4.79	4.00	2.80	22	4.9	4.8	13	5.60

[a] Calculated ionization constant of a molecule using ACD pchbat version 9.3. [b] Calculated logarithm of the octanol/water distribution coefficient at pH 7.4 using ACD pchbat version 9.3. [c] Experimentally measured bi-layer participating coefficient at pH 7.4. [d] $eLipE = -pIC_{50}(cell) - eLogD$.

The tumor growth inhibition (TGI) and the relationship to inhibition of c-Met auto-phosphorylation *in vivo* were evaluated in parallel for **8** and **9** in c-Met amplified GTL-16 xenograft tumor model. No weight loss was observed at all dose levels in the efficacy studies for both **8** and **9**. The marked efficacy results and the potential mechanisms for the tumor growth inhibition of **9** were reported previously.[16,27] Similar to **9**, **8** demonstrated dose-dependent inhibition of c-Met phosphorylation and tumor growth in the c-Met amplified GTL-16 xenograft tumor model in mice (Figure 3). Tumor regression (-34% TGI) was observed with 100 mg/kg QD group, and tumor stasis (100% TGI) was achieved with 30 mg/kg QD group. Near complete inhibition of c-Met activity for 24 hours is consistent with tumor regression and tumor stasis. The potent inhibition of c-Met activity for only a portion of the dosing schedule is consistent with the observed significant but submaximal antitumor efficacy at lower doses (10 & 3 mg/kg QD, 84% to 75% TGI). These results suggest that near-complete inhibition of c-Met autophosphorylation (>90% inhibition) for the duration of the administration schedule is necessary for maximal efficacy. The total c-Met level was not changed in the study as reported previously in the same studies of **9**.[27]
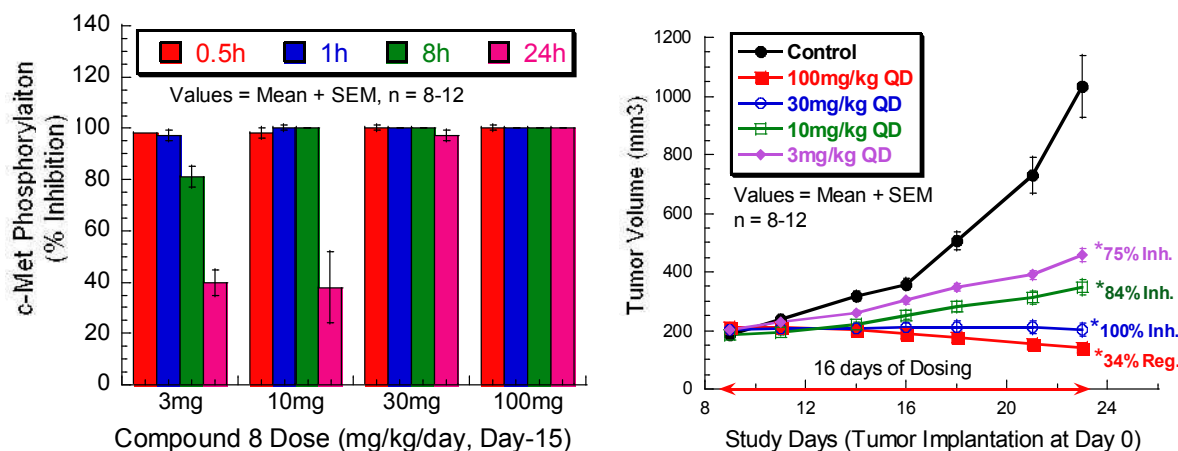
Figure 3. Inhibition of c-Met phosphorylation and tumor growth by **8** in the GTL-16 xenograft tumor model in mice.

Based on the encouraging anti-c-Met and antitumor activities *in vitro* and *in vivo*, and the desired predicted human PK properties, **8** and **9**, representing two different series were chosen for kinase selectivity and preclinical *in vitro* and *in vivo* toxicity studies. Similar to **9** which demonstrated an exquisite c-Met kinase selectivity[28], **8** is a highly kinase-selective c-Met inhibitor (>1000 selectivity to 208 protein kinases). The cocrystal structure of **8** with unphosphorylated c-Met kinase domain (Figure 4) resembles the original cocrystal structure of **7** with c-Met. As expected, the quinoline functions as a hinge binder hydrogen bound with the N-H of Met-1160. N-2 in [1,2,4]triazolo[4,3-*b*]pyridazine forms a strong hydrogen bond with N-H of Asp-1222. [1,2,4]Triazolo[4,3-*b*]pyridazine has the c-Met characteristic π-π stacking interaction with Tyr-1230, and the 6-pyrazol-4-yl group forms a coplanar with [1,2,4]triazolo[4,3-*b*]pyridazine ring to strengthen the π-π stacking interaction. C-H at C-5 position of 6-pyrazol-4yl group has a close interaction with the conserved C=O of Arg-1208, and N-2 interacts with a water molecule. As originally designed, the (*S*)-methyl group on methylene bridge is surrounded by a group of hydrophobic residues. **8** and **9** have a near completely

overlay of cocrystal structures with c-Met in both ligands and proteins (Figure 5), which supports

the exclusive kinase selectivity for both **8** and **9**.
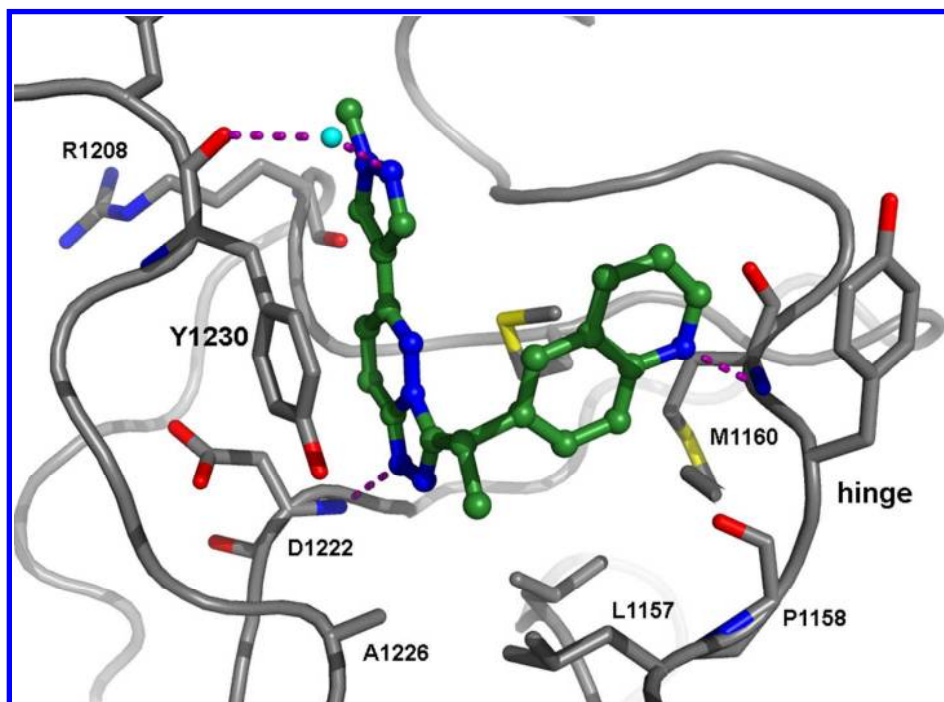
Figure 4. Cocrystal structure of **8** with c-Met unphosphorylated kinase domain (PDB 3zc5).
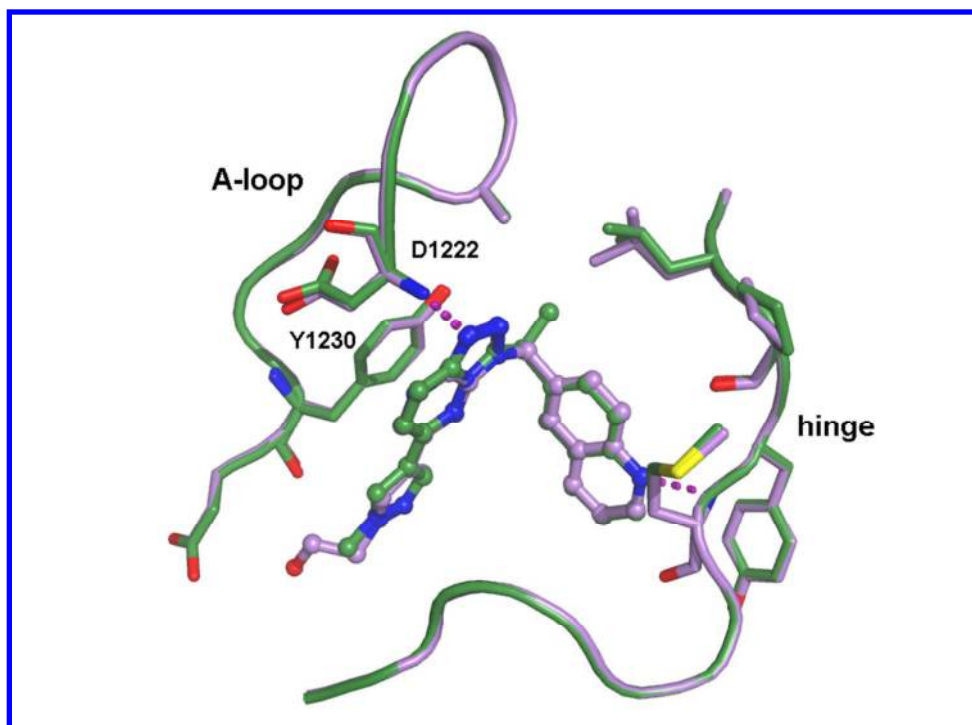
Figure 5. Overlay of cocrystal structures of **8** (green color) (PDB 3zc5) and **9** (pink color) (PDB 3zxz) with c-Met unphosphorylated kinase domain.

The interaction of the [1,2,4]triazolo[4,3-*b*]pyridazine core with the A-loop anchors the whole molecule at the ATP binding site of c-Met, which tolerates different hinge binders and substituents at 6-position. The cocrystal structure of **28F** superimposes well with **8** (Figure 6) at the [1,2,4]triazolo[4,3-*b*]pyridazine position even though **28F** has an azaindole hinge binder and an isopropylamino group at 6-position. As expected, the azaindole forms hydrogen bonds with the C=O of pro-1158 and the N-H of Met-1160 at the hinge. The alpha-methyl groups from **28F** and **8** are positioned closely in the small hydrophobic pocket. The isopropyl group in **28F** is closer to the glycine rich loop, and the N-H from the 6-isopropylamino function forms a water bridged hydrogen bond with the C=O of Arg-1208. Taken together, the cocrystal structures of c-Met reveal the specific binding characteristics of unphosphorylated c-Met protein, which allows for the design of highly selective and druggable c-Met inhibitors.
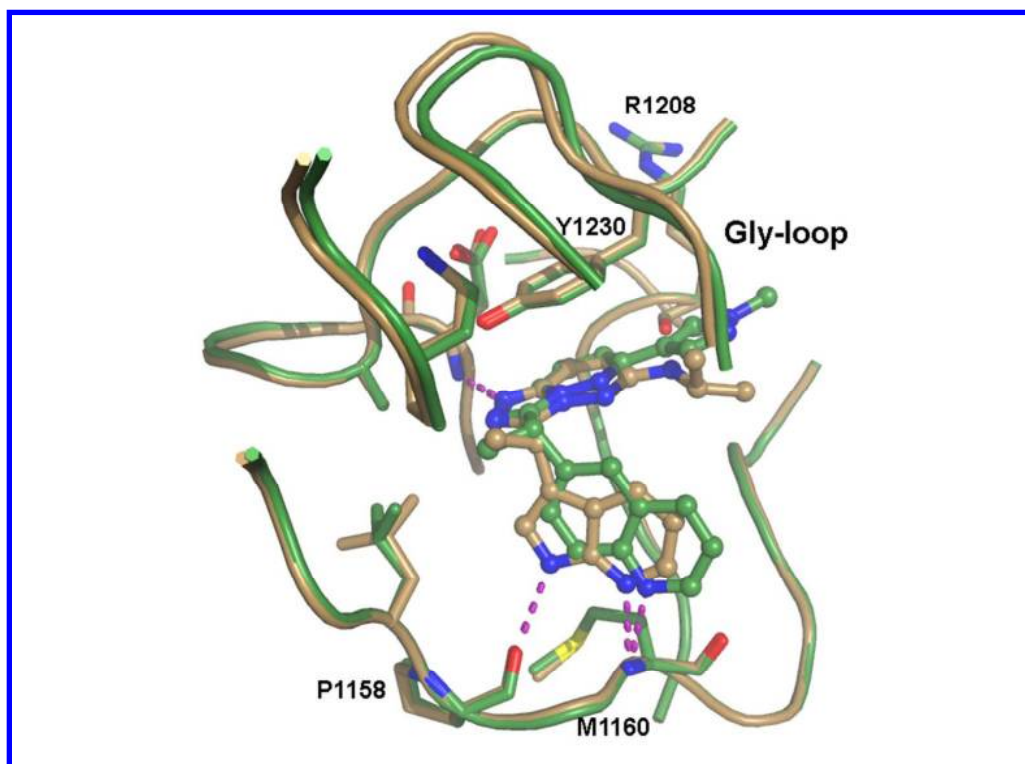
Figure 6. Superimposition of **28F** (golden color) (PDB 3zcl) with **8** (green color) (PDB 3zc5) in c-Met cocrystal structures.

Albeit the excellent selectivity to protein kinases, **8** and **9** were submitted to CEREP BioPrint (Poitiers, France) for enzymatic binding assays (68 targets) to assess the potential off-target pharmacology from inhibition of other enzyme classes (Table 5 for targets with >50% inhibition at 10 μM). Out of 68 targets, **8** had 4 hits with >50% inhibition at 10 μM, and the IC_{50}s were obtained for these targets. **8** potently inhibited GABA A BZD (IC_{50} = 0.180 μM), and PDE3 (IC_{50} = 0.170 μM). **9** was a cleaner compound with only moderate inhibition against PDE3 (IC_{50} = 1.30 μM).

Table 5. Off target hits of **8** and **9** in CEREP BioPrint screen.

	% inhibition at 10 μM	IC_{50} (μM)

Target	Compd 8	Compd 9	Compd 8	Compd 9
GABA A BZD	97	16	0.180	
Muscarinic 2	59	33	7.00	
PDE3 (h)	98	71	0.170	1.50
PDE4 (h)	63	44	3.70	

Due to the off-target activity identified in CEREP BioPrint, **8** and **9** were further evaluated in an internal Pfizer PDE assay panel including PDE1A, PDE1B, PDE1C, PDE2, PDE3A, PDE3B, PDE4A, PDE4B, PDE4C, PDE4D, PDE5, PDE6, PDE7A, PDE7B, PDE8A, PDE8B, PDE9, PDE10, and PDE11 (Table 6 for PDEs hits having IC_{50}<10 μM). **9** had weak enzymatic activities against PDE3B (5.36 μM), PDE5 (8.06 μM) and PDE10 (2.7 μM). However, **8** was unexpectedly a pan-PDE inhibitor with more potent inhibition against PDE3B (0.15 μM) and PDE10 (0.085 μM). **14C** and **15C** from the same chemistry scaffold as **8** demonstrated a similar pan-PDE inhibition profile. The introduction of the alpha-methyl group into [1,2,3]triazolo[4,5-*b*]pyrazine scaffold (**D**-series) increased the potency against c-Met and also the interactions with PDEs, as demonstrated with **8D** and **9D** (Table 6) in comparison with **9**.

Table 6. PDE family inhibition.

Compd	PDE IC_{50} (μM)									
	1A	1C	2	3A	3B	4C	4D	5	10	11
9	>10	>10	>10	>10	5.36	>10	>10	8.06	2.7	>10
8	0.58	1.4	4.56	3.53	0.15	6.7	9.61	4.89	0.085	3.03
14C	0.452	0.963	>10	2.87	0.107	2.91	2.23	1.75	0.403	2.44

15C	0.462	1.48	>10	1.8	0.088	1.97	2.06	0.287	0.432	0.963
8D	>10	>10	>10	1.25	0.699	2.08	2.5	>10	>10	>10
9D	>10	>10	>10	0.589	0.42	3.26	2.12	>10	>10	>10

The cardiovascular system controls blood pressure and beating of cardiac myocytes to accurately pump blood out of the heart to other parts of the body. These key physiological events are produced by contraction and relaxation of vascular smooth muscle and cardiac myocytes, that are regulated by intracellular cyclic nucleotide concentrations of second messengers, c-AMP and c-GMP.[29] The degradation of cyclic nucleotides is catalyzed by 3,5-cyclic nucleotide phosphodiesterases (PDEs).[29] Multiple PDEs function as a particular modulator of each cardiovascular function and regulate physiological homeostasis.[29] Therefore, inhibition of PDEs may imply a severe liability in cardiovascular safety. To further evaluate the potential cardio toxicity and other liabilities, **8** and **9** were studied in rats for finding the maximum tolerance levels. **8** in 2-, 6- or 7-day single and repeat dose rat studies resulted in a sustained increase in heart rate (HR), increased cardiac output (CO) and decreased contractility indices, as well as myocardial degeneration at dose levels ≥40 mg/kg which was equivalent to or below the predicted efficacious dose in human.[30,31] Further mechanism investigation revealed that the broad inhibition of PDE family members especially PDE3B and the activation of c-AMP may contribute to the observed cardio toxicity with **8**.[31] Consistently, the intracellular calcium and oxidative stress signaling pathways were perturbed with a dose-dependent increase in intracellular calcium following the activation of c-AMP by the treatment with **8**.[31] **8**, a pan-PDE inhibitor that was proved *in vivo* with cardio toxicity, was terminated as a pre-clinical candidate. As expected, the cardio toxicity was not observed for **9** at 42-150 fold over the predicted free

human C_{eff} of 36 nM because of a much cleaner off-target profile of **9** with only a weak inhibition against PDE3B (IC_{50} 5.36 µM).

8 and **9** from two different chemistry series, however, having the same binding mode with c-Met, were evaluated in parallel for the selection of a potential preclinical candidate. The ovrall profiles of **8** and **9** were summarized in Table S1. Both compounds demonstrated attractive potency *in vitro* and *in vivo*, exclusive kinase selectivity, good *in vitro* human ADME properties and *in vivo* rodent and dog pharmacokinetic profiles. Unexpectedly, **8** was shown to be a pan-PDE inhibitor, which might be linked with the observed *in vivo* cardio toxicity of **8** in rat. Although the protein expression levels of PDEs in *in vivo* GTL-16 tumor model were not available, a similar PK/PD relationship of **8** and **9** implied the inhibition of PDEs by **8** may not contribute significantly to the antitumor efficacy in GTL-16 c-Met-driven tumor model. Based on the overall profile, **9** was selected as a preclinical candidate for an early development evaluation, and eventually went into human phase I clinical study.[16]

CHEMISTRY

The syntheses of [1,2,4]triazolo[4,3-*b*]pyridazine compounds are summarized in Scheme I. 2-(Quinolin-6-yl)acetic acid (**31**) was synthesized from 2-(4-aminophenyl)acetic acid (**30**) using the Skraup quinoline synthesis conditions with a yield of 17.8%. After esterification, alkylation with methyl iodide in the presence of the base LDA, and hydrolysis, **32** was obtained in a combined yield of 65%. **34** was obtained in 97% yield after Boc-protection was introduced on **33**. Following methylation, removal of the Boc-group, and hydrolysis, **35** was obtained in a combined yield of 88%. The [1,2,4]triazolo[4,3-*b*]pyridazine ring was built up via the coupling reaction of **36** with the activated carboxylic acid, and followed by heating under an acidic

condition to afford **38**. A variety of substituents were introduced at 6-position of **38** via the

conventional Suzuki coupling reaction or replacement of chloride with amino groups.

Scheme I[a]. Syntheses of [1,2,4]triazolo[4,3-*b*]pyridazine compounds.
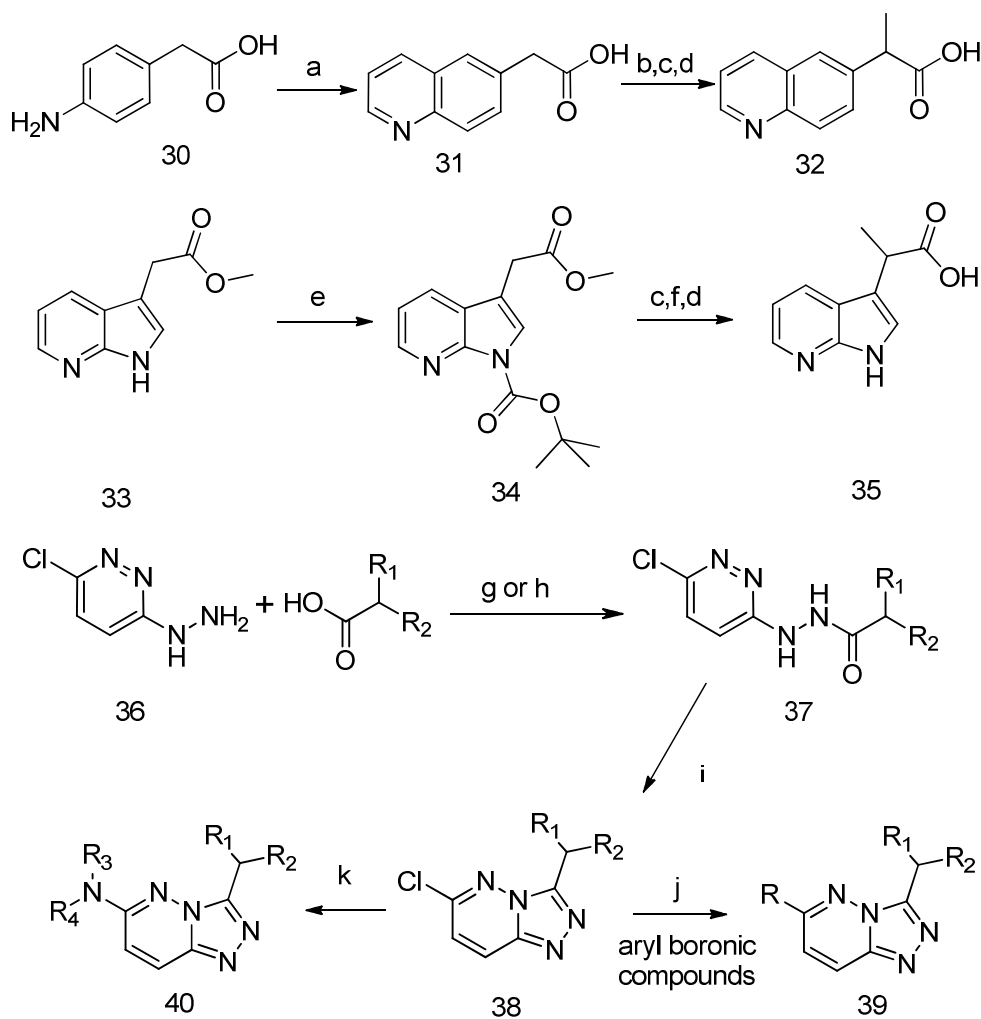
38A: R$_1$ = H, R$_2$ = 6-quinolinyl
38C: R$_1$ = CH$_3$, R$_2$ = 6-quinolinyl
38E: R$_1$ = H, R$_2$ = 1*H*-pyrrolo[2,3-*b*]pyridin-3-yl
38F: R$_1$ = CH$_3$, R$_2$ = 1*H*-pyrrolo[2,3-*b*]pyridin-3-yl

[a] Reagents and conditions: (a) glycerol/FeSO$_4$/conc.H$_2$SO$_4$, nitrobenzene, reflux, 5 h. (b) SOCl$_2$, Methanol, reflux. (c) LDA/MeI, anhydrous THF, -78 ^{o}C to ambient temperature, overnight. (d) LiOH, MeOH/H$_2$O, 65 ^{o}C, 4 h. (e) (Boc)$_2$O/DMAP, THF, overnight. (f) HCl/Dioxane (4N), CH$_2$Cl$_2$. (g) EDC or HATU, DMF, overnight. (h) SOCl$_2$, DMF, 100 ^{o}C, 30 min. (i) Acetic acid, reflux, 2 h. (j) Pd(dppf)Cl$_2$·CH$_2$Cl$_2$, Cs$_2$CO$_3$, DME/H$_2$O, 80 ^{o}C, overnight. (k) amine, *n*-Butanol, microwave at 125 ^{o}C, ~1 h.

The syntheses of (*S*)-6-(1-(1*H*-[1,2,3]triazolo[4,5-*b*]pyrazin-1-yl)ethyl)quinoline compounds are summarized in Scheme II. **47** was prepared with a four-step procedure. Quinoline-6-carboxylic acid **41** reacted with *N,O*-dimethyl hydroxylamine in the presence of the activation reagent CDI in DMF to afford **42** in 97% yield, which reacted with MeMgCl to provide the ketone **43** in 97% yield, and followed by amination and hydrogenation to provide **45** in 97% yield. The thermal replacement of 2-bromo in **46** with **45** were accomplished in *n*-butanol in the presence of DIPEA after microwaving at 225 $^{\circ}$C for 1 h to afford **47** in 66% yield. The [1,2,3]triazolo[4,5-*b*]pyrazine ring was constructed with isoamyl nitrile in DMF at 0 $^{\circ}$C and then at 70 $^{\circ}$C for 1 h to afford **48** in 72% yield. The racemic **48** was purified on a chiral SFC column using MeOH and liquid CO_2 as elution system to provide **49** and **50**. The absolute configuration of **49** was determined by the x-ray cocrystal structure with c-Met. A variety of compounds were made using the chiral intermediate **49** via the conventional Suzuki coupling reaction.

Scheme II^{a}. Syntheses of (*S*)-6-(1-(1*H*-[1,2,3]triazolo[4,5-*b*]pyrazin-1-yl)ethyl)quinoline compounds
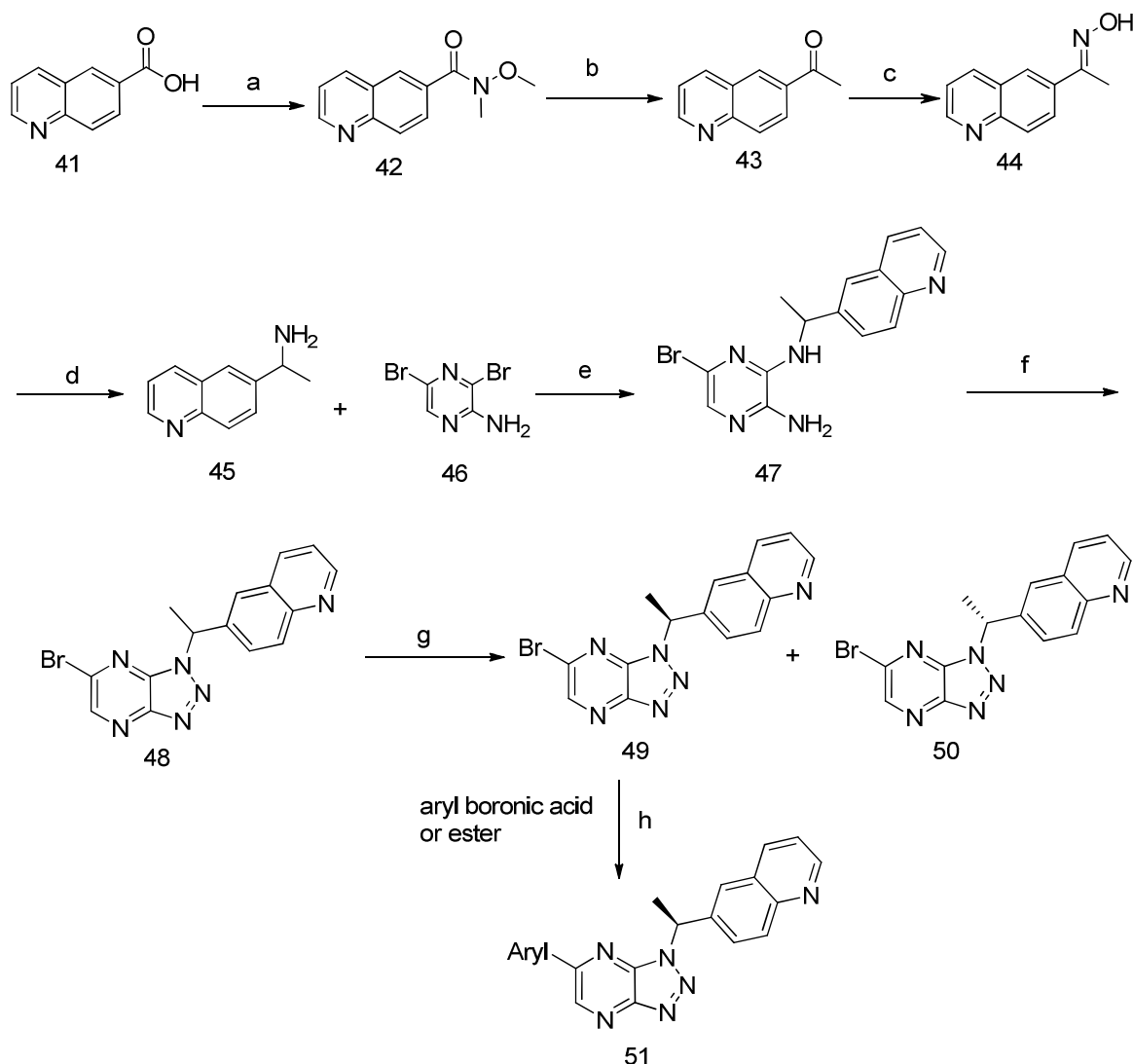
^{a} Reagents and conditions: (a) MeNHOMe/CDI, DMF, ambient temperature, overnight. (b) MeMgBr, anhydrous THF, 0 ^{o}C to ambient temperature, 16 h. (c) NH$_2$OH·HCl/NaOH, ethanol, 16 h. (d) 7N NH$_3$ in methanol, EtOH, H$_2$, Raney nickel, 16 h. (e) DIPEA, n-BuOH, microwave at 225 ^{o}C, 1 h. (f) isoamyl nitrile, DMF, 70 ^{o}C, 1 h. (g) chiral separation on a chiral SFC column using MeOH and liquid CO$_2$ as elution system. (h) Pd(dppf)Cl$_2$·CH$_2$Cl$_2$, Cs$_2$CO$_3$, DME/H$_2$O, 80 ^{o}C, overnight.

CONCLUSIONS

Receptor tyrosine kinases (RTKs) play fundamental roles in cell proliferation, migration, metabolism, differentiation, and survival. Alterations in the normal functions of protein kinases are linked with the pathological changes within cell that leads to diseases. The constitutively enhanced RTK activities have been implicated in the development and progression of many

types of cancer.[32] Since the first approval of ABL protein kinase inhibitor Gleevec for the treatment of chronic myeloid leukemia patients with *BCR-ABL* abnormal gene in 2001, a number of RTK inhibitors have been successfully discovered and developed against the aberrant RTK signaling in various cancers, including sunitinib and axitinib for targeting the VHL-dependent VEGF pathway in renal cell carcinoma, erlotinib and gefitinib targeting EGFR in non-small cell lung cancer (NSCLC) with mutant EGFR, and crizotinib targeting c-Met, Alk and Ros in NSCLC. The discovery and development of highly selective kinase inhibitors have been challenging because of the similarity of the protein kinase ATP binding sites. Most of the kinase inhibitor drugs approved for cancer treatments are multi-target kinase inhibitors and suffer side effects which limit their utility. From a highly specific HTS hit, we have discovered two c-Met inhibitors **8** and **9** exhibiting exquisite kinase selectivity as well as many attractive properties. During the broad ligand off-target screens, it was discovered that **8** was a pan-PDE family inhibitor, which was correlated to a sustained increase in heart rate, increased cardiac output, and decreased contractility indices, as well as myocardial degeneration in *in vivo* safety evaluations in rats. **8** was terminated as a preclinical candidate because of narrow therapeutic window in cardio-related safety. **9**, which has a higher LipE value for c-Met compared to **8** (7.02 vs 6.17) demonstrated a more selective profile in the broad ligand off-target screen, and a large therapeutic window in *in vivo* animal tolerance studies. **9** was selected as a preclinical candidate and later entered human clinical evaluations for cancer treatment. These findings reinforce the need for broad preclinical evaluations to identify a more complete range of affected pharmacology.

The attrition rate for drug development is rising, and late phase attrition remains high, which contributes to an unsustainable increase in R&D spending.[33] Although there are several factors

that contribute to attrition, one of the major reasons is toxicity. 40% of NCEs that begin preclinical safety studies in animals fail due to toxicity.[34] It is important to establish *in vitro* toxicity models to predict human *in vivo* toxicity, and identify issues at early drug discovery stages. Broad off-target screening is one effective way to profile compounds at various stages and alert chemists to potential issues that can be addressed during optimization. Although both **8** and **9** have exquisite kinase selectivity for c-Met, and desired *in vitro* ADME and *in vivo* PK properties, the off-target inhibition of members of the PDE family by compound **8** caused severe cardio toxicity in rats. **8** was terminated at the early stage. It is challenging to design compounds with a completely clean profile in the off-target screens. LipE has been proposed as an index that may have some correlation with a good toxicity profile.[35] Indeed, **9** with a higher c-Met cell LipE value than **8** (7.02 vs 6.17, respectively) demonstrated a much better profile in broad ligand screens leading to good safety profile in *in vivo* preclinical animal studies. Therefore, **9** was selected for early development. One of the major challenges in drug discovery is to identify a compound with a good balanced profile in biological functions and physicochemical properties. It is important at the early stage of drug discovery to establish an effective screen cascade for multi-parameter optimizations, and identify the key ADME and safety issues associated with the selected chemistry scaffolds. Optimization of multiple chemistry series, or at least two chemical series, is highly recommended to avoid late attrition of the project because of toxicity. Parallel optimization of both triazolopyrazine and triazolopyridazine series overcame the preclinical cardio toxicity from the triazolopyridazine series and successfully selected **9** from the triazolopyrazine series into human clinical trials without a significant delay of the project progression.

EXPERIMENTAL SECTION

General Methods for Chemistry. All reagents and solvents were used as purchased from commercial sources. Reactions were carried out under nitrogen atmosphere unless otherwise indicated. Silica gel chromatography was done using the appropriate size Biotage® pre-packed silica filled cartridges. NMR spectra were generated on a Bruker 300 or 400 MHz instrument and obtained as CDCl$_3$ or DMSO-d_6 or MeOH-d_4 solutions (reported in ppm), using CDCl$_3$ as the reference standard (7.27 ppm), DMSO-d_6 (2.50 ppm), and MeOH-d_4 (3.31 ppm). Multiplicities were given as s (singlet), b. s. (broad singlet), d (doublet), t (triplet), dt (double of triplets), and m (multiplet). Mass spectral data (APCI) was gathered on an Agilent 1100 LC with MSD (Agilent model G1946B upgraded to D model) single-quadrupole mass spec detectors running with atmospheric pressure chemical ionization source. The LC instrument includes a binary pump (Agilent model G1312A) with upper pressure limit of 400 bar attached to autosampler (Agilent model G1313A) which uses external tray for sample submission. The column compartment (Agilent model G1316A) is attached to diode array (Agilent model G1315A). The instrument acquisition and data handling was done with ChemStation rev. B.02.01. The Purity measurements were done by measuring peak area at 254nm, 224nm and total ion chromatogram. To evaluate the purity of each peak UV-Vis spectrum from 190-700 nm at step size of 2 nm and mass spectrum scan from 150-850 amu with cycle time of 0.29 cycle/sec was performed. Retention times (RT) were in minutes and purity was calculated as percentage of total area. Two HPLC methods were utilized for purity. Method A: Waters Acquity UPLC BEH C18 column, 1.7μm, 2.1x100 mm, column temperature 80 °C; solvent A: water (0.1% formic acid and 0.05% ammonium formate); solvent B: methanol (0.1% formic acid and 0.05% ammonium formate); gradient: 5-95 % B in 10 min, 95% B 10-12 min; Flow rate 0.6 mL/min. Method B: EclipsXDB C8 column, 3.5 μm, 4.6x50 mm, column temperature 40 °C; solvent A:

water (5% ACN, 2mM ammonium acetate, 0.1% acetic acid); solvent B: ACN (5% H_2O, 2mM ammonium acetate, 0.1% acetic acid); gradient: 20-85 B% (0.0-2.5min), 85-95 B% (2.5-3.5min), 95 B% (5min); Flow Rate = 0.8 mL/min. Compound purity was determined by combustion analysis (Atlantic Microlabs, Inc.) or high pressure liquid chromatography (HPLC) with a confirming purity of ≥ 95% for all of final biological testing compounds.

2-(Quinolin-6-yl)acetic acid (31). A mixture of 2-(4-aminophenyl)acetic acid (276 g, 1.8 mol), ferrous sulfate (63.6 g, 0.22 mol), glycerol (696 g, 7.56 mol), nitrobenzene (138 g, 1.12 mol) and concentrated sulfuric acid (324 mL) was heated gently. After the first vigorous reaction, the mixture was refluxed for five hours and then was treated with aq. sodium hydroxide solution (2 N, 1320 mL), stirred with kieselguhr, and filtered. The filtrate was basified with aq. sodium hydroxide solution to pH 5−6, and a dark brown precipitate formed. The precipitate was filtered, washed with water, taken up with aq. sodium hydroxide solution (0.82 N, 3000 mL), then boiled with carbon (150 g). The mixture was filtered and the filtrate was treated with glacial acetic acid (240 mL), and the mixture was left standing overnight during which time dark-brown crystalline precipitate formed. The precipitate was collected and dried in vacuum to give **31** (60 g, 17.8%). LC-MS m/z (M-1)$^-$ 186; ^{1}H NMR (400 MHz, DMSO-d_6) δ 12.53 (br. s, 1H), 8.87 (dd, J = 4.29, 1.77 Hz, 1H), 8.30−8.35 (m, 1H), 7.97 (d, J = 8.59 Hz, 1H), 7.84 (d, J = 1.52 Hz, 1H), 7.68 (dd, J = 8.59, 2.02 Hz, 1H), 7.52 (dd, J = 8.21, 4.17 Hz, 1H), 3.80 (s, 2H).

2-(Quinolin-6-yl)propanoic acid (32). To a suspension of **31** (60 g, 0.32 mol) in MeOH (600 mL) cooled to 0−5 °C, $SOCl_2$ (30 mL, 0.35 mol) was added dropwise. After the mixture was heated to reflux for 2 h, the mixture was evaporated under reduced pressure, and the residue was taken up with EtOAc (600 mL). The mixture was washed with aq. $NaHCO_3$ and brine, dried over Na_2SO_4 and concentrated to give crude methyl ester, which was purified via a silica column

chromatography (EtOAc: petroleum ether = 1:5) to give methyl 2-(quinolin-6-yl)acetate (50 g, 72.6%) as a yellow oil. To a solution of methyl 2-(quinolin-6-yl)acetate (20.00 g, 99.54 mmol) in anhydrous tetrahydrofuran (200 mL) was added LDA (1.8 M THF solution, 61 mL, 109.5 mmol) dropwise at -78 °C under nitrogen. The reaction mixture was stirred at -78 °C under nitrogen for half an hour. To the reaction mixture was added methyl iodide (6.20 mL, 99.54 mmol), and the mixture was stirred under nitrogen from -78 °C to ambient temperature overnight. The reaction was quenched with the careful addition of water. The product was extracted with ethyl acetate. The combined extracts were washed with water and brine, dried over Na_2SO_4, and concentrated to provide methyl 2-(quinolin-6-yl)propanoate (21.49 g, ~100% yield). To a solution of 2-(quinolin-6-yl)propanoate (21.17 g, 98.35 mmol) in methanol (200 mL) and water (50 mL) was added lithium hydroxide (12.02 g, 491.75 mmol). The reaction mixture was stirred at 65 °C oil bath for 4 hours, cooled to ambient temperature, and adjusted the acidity to pH ~7 with 6N HCl (65 mL). A lot of precipitate was formed. After filtration, the solid was washed with water, and the filtrate was concentrated to remove methanol. The solid was filtrated and washed with water. The combined solid product was dried under high vacuum to provide **32** (19.09 g, 90% yield). LC-MS *m/z* (M+1)$^+$ 202; ^{1}H NMR (400 MHz, DMSO-d_6) δ 8.78 (dd, *J* = 4.04, 1.77 Hz, 1H), 8.20−8.26 (m, 1 H), 7.82−7.89 (m, 1H), 7.72−7.80 (m, 2H), 7.43 (dd, *J* = 8.34, 4.04 Hz, 1H), 3.54 (q, *J* = 7.07 Hz, 1H), 1.37 (d, *J* = 7.07 Hz, 3H).

2-(1*H*-Pyrrolo[2,3-*b*]pyridin-3-yl)propanoic acid (35). To a solution of methyl (1*H*-pyrrolo[2,3-*b*]pyridin-3-yl)-acetate (5.10 g, 28.78 mmol) and 4-dimethylaminopyridine (175.8 mg, 1.44 mmol) in anhydrous THF (100 mL) was added di-tertbutyldicarbonate (34.6 g, 34.54 mmol). The reaction mixture was stirred for overnight, diluted with ethyl acetate, washed with water and brine, dried over Na_2SO_4, and concentrated. The residue was suspended in hexane,

and the solid was filtered and dried to provide a white solid of 3-methoxycarbonylmethyl-pyrrolo[2,3-*b*]pyridine-1-carboxylic acid tert-butyl ester (6.07 g). The filtrate was concentrated and purified on a silica gel column eluting with hexane-ethyl acetate to provide additional product (1.71 g, total 7.78 g, 97% yield). ^{1}H NMR (400 MHz, CHLOROFORM-D) δ 8.38 (dd, *J* = 4.55, 1.52 Hz, 1H), 7.99 (dd, *J* = 7.83, 1.52 Hz, 1H), 7.73 (s, 1H), 7.28 (dd, *J* = 7.83, 4.80 Hz, 1H), 3.83 (s, 2H), 3.62 (s, 3H), 1.60 (s, 9H).

To a solution of 3-methoxycarbonylmethyl-pyrrolo[2,3-b]pyridine-1-carboxylic acid *tert*-butyl ester (6.07 g, 20.9 mmol) in anhydrous THF (100 mL) was added LDA (1.8 M THF solution, 12.7 mL, 22.99 mmol) at -78 °C under nitrogen. The reaction mixture was stirred at -78 °C under nitrogen for half an hour and then methyl iodide was added. The reaction mixture was stirred from -78 °C to ambient temperature overnight under nitrogen, quenched with an addition of saturated ammonium chloride, and diluted with ethyl acetate. The ethyl acetate layer was washed with brine, dried over Na_2SO_4, concentrated, and dried under high vacuum to provide 3-(1-methoxycarbonyl-ethyl)-pyrrolo[2,3-*b*]pyridine-1-carboxylic acid *tert*-butyl ester (6.35 g, ~100% yield).   To a solution of 3-(1-methoxycarbonyl-ethyl)-pyrrolo[2,3-*b*]pyridine-1-carboxylic acid *tert*-butyl ester (6.35 g, 20.9 mmol) in dichloromethane (50 mL) was added HCl dioxane solution (4N, 20 mL). The reaction mixture was stirred for overnight. After evaporation and high vacuum dry, the product was used directly for the next step. To a solution of methyl 2-(1*H*-pyrrolo[2,3-*b*]pyridin-3-yl)-propionate (4.26 g, 20.9 mmol) in methanol (45 mL) and water (15 mL) was added LiOH (2.503 g, 104.5 mmol). The reaction mixture was stirred at 60 °C oil bath for 2 hours. After cooling, the reaction mixture was neutralized to pH ~6 with 6N HCl solution. The solid was filtered and washed with water to provide **35** (2.45 g). The filtrate was

concentrated and purified on a reverse-phase C-18 preparative HPLC to provide another portion

of **35** (1.05 g, total 3.50 g).

(S)-6-(1-(6-Chloro-[1,2,4]triazolo[4,3-b]pyridazin-3-yl)ethyl)quinoline   (38C).   To   a

solution of **32** (3.00 g, 14.9 mmol) in DMF (75 mL) was added 1-(3-dimethylaminopropyl)-3-

ethylcarbodiimide hydrochloride (3.14 g, 16.4 mmol). The reaction mixture was stirred under

nitrogen for half an hour and then (6-chloro-pyridazin-3-yl)-hydrazine (2.22 g, 14.9 mmol) was

added. The reaction mixture was stirred under nitrogen for overnight, diluted with ethyl acetate,

washed with water, dried over Na_2SO_4, and concentrated to get the crude intermediate, which

was dissolved in acetic acid (20 mL). The acetic acid solution was refluxed for 2 hours, and

concentrated. The residue was purified on a silica gel column eluting with 5% methanol in ethyl

acetate to provide   6-[1-(6-chloro-[1,2,4]triazolo[4,3-b]pyridazin-3-yl)-ethyl]-quinoline (1.16 g,

25% yield). The racemic compound was resolved with a chiral column (Chiralcel AD-H) eluting

with 45% methanol in liquid carbon dioxide (100 bar, 2.5 mL/min).   (R)-6-[1-(6-chloro-

[1,2,4]triazolo[4,3-b]pyridazin-3-yl)-ethyl]-quinoline had an optical rotation of +0.157° in

methanol (5.53   mg/mL),   and   (S)-6-[1-(6-chloro-[1,2,4]triazolo[4,3-b]pyridazin-3-yl)-ethyl]-

quinoline (**38C**) had an optical rotation of -0.125° in methanol (5.22 mg/mL). The absolute

configuration was proved with a cocrystal structure with c-Met. LC-MS m/z $(M+1)^+$ 310, 312;

^{1}H NMR (400 MHz, DMSO-d_6) δ 1.89 (d, J = 7.33 Hz, 3H), 5.00 (q, J = 7.07 Hz, 1H), 7.46 (d, J

= 9.60 Hz, 1H), 7.51 (dd, J = 8.34, 4.29 Hz, 1H), 7.78 (dd, J = 8.84, 2.02 Hz, 1H), 7.87 (d, J =

1.77 Hz, 1H), 7.98 (d, J = 8.84 Hz, 1H), 8.33 (d, J = 8.34 Hz, 1H), 8.45 (d, J = 9.60 Hz, 1H),

8.86 (dd, J = 4.17, 1.64 Hz, 1H).

6-((6-Chloro-[1,2,4]triazolo[4,3-b]pyridazin-3-yl)methyl)quinoline   (38A).   38A   was

prepared with the same method as **38C**.   LC-MS m/z $(M+1)^+$ 295, 297; ^{1}H NMR (400 MHz,

DMSO-d_6) δ 8.86 (dd, J = 1.65, 4.22 Hz, 1H), 8.46 (d, J = 9.66 Hz, 1H), 8.27−8.34 (m, 1H), 7.98 (d, J = 8.56 Hz, 1H), 7.86 (d, J = 1.47 Hz, 1H), 7.74 (dd, J = 1.96, 8.68 Hz, 1H), 7.45−7.53 (m, 2H), 4.71 (s, 2H).

3-((1*H*-Pyrrolo[2,3-*b*]pyridin-3-yl)methyl)-6-chloro-[1,2,4]triazolo[4,3-*b*]pyridazine (38E). To a solution of (1*H*-pyrrolo[2,3-*b*]pyridin-3-yl)-acetic acid (283 mg, 1.61 mmol) and (6-chloro-pyridazin-3-yl)-hydrazine (233 mg, 1.61 mmol) in DMF (8 mL) was added HATU (612 mg, 1.61 mmol). The reaction mixture was stirred at ambient temperature for one hour and then heated at 120 °C for two hours. After cooling, the reaction was concentrated and purified on a reverse-phase C-18 preparative HPLC eluting with acetonitrile-water containing 0.1% acetic acid to provide **38E** (99 mg, 20% yield). LC-MS *m/z* (M+1)$^+$ 285, 287; ^{1}H NMR (400 MHz, DMSO-d_6) δ 11.68 (s, 1H), 8.36−8.53 (m, 1H), 8.23 (d, J = 4.80 Hz, 1H), 8.03−8.13 (m, 1H), 7.40−7.51 (m, 2 H), 7.11 (dd, J = 7.83, 4.80 Hz, 1H), 4.59 (s, 1H).

(*S*)-3-(1-(1*H*-Pyrrolo[2,3-*b*]pyridin-3-yl)ethyl)-6-chloro-[1,2,4]triazolo[4,3-*b*]pyridazine (38F). The suspension of **35** (542 mg, 2.85 mmol) in thionyl chloride (6 mL) was stirred at ambient temperature for two hours, and then thionyl chloride was removed in vacuo. To the residue was added a solution of (6-chloro-pyridazin-3-yl)-hydrazine (412 mg, 2.85 mmol) in anhydrous DMF (5 mL). The reaction solution was stirred for 5 minutes at ambient temperature and then heated at 100 °C oil bath for 30 minutes. After cooling, DMF was removed with vacuum. The residue was dissolved in water, washed with ethyl acetate, and the water layer was lyophilized to provide 6-chloro-3-[1-(1*H*-pyrrolo[2,3-*b*]pyridin-3-yl)-ethyl]-[1,2,4]triazolo[4,3-*b*]pyridazine (610 mg, 71.5% yield). The racemic compound was resolved on a chiral SFC column using MeOH and liquid CO_2 as elution system to provide **38F.** The absolute configuration of **38F** was determined by a cocrystal structure with c-Met. LC-MS *m/z* (M+1)$^+$

310, 312; ^{1}H NMR (400 MHz, DMSO-d_6) δ 8.86 (dd, J = 4.17, 1.64 Hz, 1H), 8.45 (d, J = 9.60 Hz, 1H), 8.33 (d, J = 8.34 Hz, 1H), 7.98 (d, J = 8.84 Hz, 1H), 7.87 (d, J = 1.77 Hz, 1H), 7.78 (dd, J = 8.84, 2.02 Hz, 1H), 7.51 (dd, J = 8.34, 4.29 Hz, 1H), 7.46 (d, J = 9.60 Hz,1H), 5.00 (q, J = 7.33 Hz, 1H), 1.89 (d, J = 7.33 Hz, 3H).

(*S*)-6-(1-(6-Bromo-1*H*-[1,2,3]triazolo[4,5-*b*]pyrazin-1-yl)ethyl)quinoline (49).

Step 1.   To a solution of **41** (10g, 57.75 mmol) in DMF (200 mL) was added carbonyl diimidazole (10.3 g, 62.5 mmol) under nitrogen.   The reaction was stirred for 1 h.   To the solution was added *N,O*-dimethyl hydroxylamine (5.6 g, 57.75 mmol), and the reaction was stirred at ambient temperature for 16 h.   The reaction was diluted with EtOAc (150 mL) and water (150 mL).   The organic layer was separated, and the aqueous layer was extracted with EtOAc (5 x 100 mL).   The organics were combined and washed with water (3 x 100 mL), brine (2 x 100 mL), dried over Na_2SO_4, filtered and concentrated to give **42** (11.97 g, 97% yield).

Step 2. To a solution of **42** (11.97g, 55.35 mmol) in anhydrous THF (200 mL) was added MeMgBr (1.5 M in THF, 55 mL, 83 mmol) at 0 °C under nitrogen.   The reaction was allowed to warm to ambient temperature over 16 h.   Saturated NH_4Cl (20 mL) was added to quench the reaction.   The reaction solution was then extracted with EtOAc (3 x 50 mL).   The combined organics were dried over Na_2SO_4, filtered, and concentrated to give **43** (9.2 g, 97% yield).

Step 3. To a suspension of hydroxylamine hydrochloride in EtOH (150 mL) was added a suspension of NaOH (2.4 g, 59.7 mmol) in EtOH (25 mL).   The reaction mixture was stirred at ambient temperature for 15 min.   The precipitated sodium hydrochloride was filtered off.   A solution of 1-quinolin-6-yl-ethanone (9.3 g, 54.25 mmol) in EtOH (150 mL) was added.   The reaction solution was stirred for 16 hours at ambient temperature.   EtOH was removed in vacuum to give **44** (10.1 g, >99% yield).

Step 4. To a solution of **44** (4.54 g, 24.4 mmol) in EtOH (50 mL) was added methanol solution of NH_3 (7N, 12 mL, 80 mmol). A slurry of Raney nickel (washed 3 x with EtOH) about 2 g was added followed by a hydrogen-filled balloon. The reaction was stirred at ambient temperature for 16 hours under hydrogen-filled balloon. The reaction mixture was filtered over a pad of celite and the mother liquor was concentrated to give quantitative **45** (4.1 g, 97.6%).

Step 5. To a solution of 2-amino-dibromopyrazine (5.1 g, 20 mmol) and **45** (3.43 g, 20 mmol) in *n*-BuOH (5 mL) was added diisopropylethylamine (10.5 mL, 60 mmol). The reaction was irradiated in a microwave at 225 ^{o}C for 1 hour. The reaction mixture was concentrated and purified by column chromatography Biotage 40+M 0-50% EtOAc:Hexanes (7 column volumes), 50-100% (10 column volumes), and EtOAc with 10% MeOH to give **47** (2.1 g, 66%).

Step 6. To a solution of **47** in anhydrous DMF (25 mL) was added isoamyl nitrile (0.98 mL, 1.2 mmol) at 0 ^{o}C. The reaction was stirred at 0 ^{o}C for 5 min, then the ice bath was removed and allowed to stir at ambient temperature for 5 min. The reaction was then heated at 70 ^{o}C for 1 hour, cooled and quenched with sat. aqueous solution of Na_2SO_3 (10 mL). Water (50 mL) and EtOAc (50 mL) were added. The organic layer was separated and the aqueous layer was extracted with EtOAc (4 x 100 mL). The combined organics were washed with $NaHCO_3$ (50 mL) and water (3 x 50 mL), dried over Na_2SO_4, filtered and concentrated to give **48** (1.56 g, 72% yield).

Step 7. The racemic **48** was resolved on a chiral SFC column using MeOH and liquid CO_2 as elution system to provide **49** and **50**. The absolute configuration of 49 was determined by a cocrystal structure with c-Met. LC-MS *m/z* (M+1)$^{+}$ 354, 356; ^{1}H NMR (400 MHz, DMSO-d_6) 1H NMR (300 MHz, DMSO-d_6) δ ppm 8.99 (s, 1H), 8.90 (dd, *J* = 4.14, 1.70 Hz, 1H), 8.38 (d, *J*

= 8.10 Hz, 1H), 7.97−8.07 (m, 2H), 7.76−7.88 (m, 1H), 7.54 (dd, J = 8.38, 4.24 Hz, 1H), 6.45−6.73 (q, J = 6.97 Hz, 1H), 2.19 (d, J = 6.97 Hz, 3H).

General Procedure A for Suzuki coupling reaction.

(*S*)-4-(3-(1-(Quinolin-6-yl)ethyl)-[1,2,4]triazolo[4,3-*b*]pyridazin-6-yl)benzonitrile (16C). To a solution of **38C** (50 mg, 0.16 mmol) and 4-cyanophenyl boronic acid (26.4 mg, 0.18 mmol) in 1,2-dimethoxyethane (1.5 mL) was added a freshly prepared solution of Cs_2CO_3 (186.3 mg, 0.528 mmol) in water (0.5 mL), and the catalyst Pd(dppf)Cl$_2$.CH$_2$Cl$_2$ (6.5 mg, 0.008 mmol). The reaction mixture was degassed and charged with nitrogen for three times, and heated at 80 ^{o}C oil bath overnight. The reaction solution was diluted with methanol, and filtered through a celite pad. The filtrate was concentrated and purified on a reverse-phase C-18 preparative HPLC eluting with acetonitrile-water containing 0.1% acetic acid to provide **16C** (27 mg, 45% yield). LC-MS m/z (M+1)$^+$ 377; ^{1}H NMR (400 MHz, DMSO-d_6) δ 8.84 (d, J = 2.69 Hz, 1H), 8.49 (d, J = 9.78 Hz, 1H), 8.35 (d, J = 8.44 Hz, 1H), 8.23 (d, J = 8.31 Hz, 2H), 8.04 (d, J = 8.31 Hz, 2H), 7.95−8.02 (m, 3H), 7.84 (d, J = 8.68 Hz, 1H), 7.45−7.53 (m, 1H), 5.11−5.23 (m, J = 7.00 Hz, 1H), 1.96 (d, J = 7.21 Hz, 3H); HPLC purity (method A): RT 5.717, >95%.

Compounds of 6-aryl-[1,2,4]triazolo[4,3-*b*]pyridazines and 6-aryl-1*H*-[1,2,3]triazolo[4,5-*b*]pyrazines were prepared according to the General Procedure A.

6-((6-(3,4-Difluorophenyl)-[1,2,4]triazolo[4,3-*b*]pyridazin-3-yl)methyl)quinoline (14A). LC-MS m/z (M+1)$^+$ 374; ^{1}H NMR (400 MHz, DMSO-d_6) δ 8.85 (dd, J = 4.17, 1.64Hz, 1H), 8.46 (d, J = 9.85Hz, 1H), 8.28−8.34 (m, 1H), 8.14−8.24 (m, 1H), 7.93−8.05 (m, 3H), 7.80 (dd, J = 8.72, 1.89 Hz, 1H), 7.60−7.71 (m, 1H), 7.50 (dd, J = 8.34, 4.29Hz, 1H), 7.21 (d, J = 4.80Hz, 1H), 4.82 (s, 2H); HPLC purity (method A): RT 6.401, >95%.

3-(3-(Quinolin-6-ylmethyl)-[1,2,4]triazolo[4,3-*b*]pyridazin-6-yl)benzonitrile (15A).   LC-MS *m/z* (M+1)$^+$ 342; ^{1}H NMR (400 MHz, DMSO-d$_6$) δ 8.87 (dd, *J* = 4.14, 1.70 Hz, 1H), 8.60 (s, 1H), 8.52 (d, *J* = 9.80 Hz, 1H), 8.43−8.49 (m, 1H), 8.33 (d, *J* = 0.94 Hz, 1H), 7.97−8.11 (m, 4H), 7.78−7.87 (m, 2H), 7.52 (dd, *J* = 8.29, 4.33 Hz, 1H), 4.86 (s, 2H); HPLC purity (method A): RT 5.297, 99.1%.

4-(3-(Quinolin-6-ylmethyl)-[1,2,4]triazolo[4,3-*b*]pyridazin-6-yl)benzonitrile (16A).   LC-MS *m/z* (M+1)$^+$ 363; ^{1}H NMR (400 MHz, DMSO-*d$_6$*) δ 8.87 (dd, *J* = 1.71, 4.16 Hz, 1H), 8.52 (d, *J* = 9.78 Hz, 1H), 8.28−8.38 (m, 3H), 7.94−8.12 (m, 5H), 7.83 (dd, *J* = 1.96, 8.80 Hz, 1H), 7.52 (dd, *J* = 4.28, 8.31 Hz, 1H), 4.85 (s, 2H); HPLC purity (method A): RT 6.160, >95%.

6-((6-(1-Methyl-1*H*-pyrazol-4-yl)-[1,2,4]triazolo[4,3-*b*]pyridazin-3-yl)methyl)quinoline (17A). LC-MS m/z (M+1)$^+$ 342; ^{1}H NMR (400 MHz, DMSO-*d$_6$*) δ 8.84 (dd, *J* = 4.24, 1.60 Hz, 1H), 8.52 (s, 1H), 8.26−8.39 (m, 2H), 8.16 (s, 1H), 7.93−8.03 (m, 2H), 7.73−7.86 (m, 1H), 7.67 (d, *J* = 9.61 Hz, 1H), 7.50 (dd, *J* = 8.29, 4.33 Hz, 1H), 4.73 (s, 2H), 3.93 (s, 3H); HPLC purity (method A): RT 4.238, >99%.

(*S*)-6-(1-(6-(3,4-Difluorophenyl)-[1,2,4]triazolo[4,3-*b*]pyridazin-3-yl)ethyl)quinoline (14C). LC-MS *m/z* (M+1)$^+$ 388; ^{1}H NMR (400 MHz, DMSO-*d$_6$*) δ 8.84 (dd, *J* =4 .29, 1.77 Hz, 1H), 8.45 (d, *J* = 9.60 Hz, 1H), 8.35(d, *J* = 7.58 Hz, 1H), 8.03−8.11 (m, 1H), 7.97−8.02 (m, 2H), 7.95 (d, *J* = 4.04 Hz, 1H), 7.89−7.93 (m, 1H), 7.82 (dd, *J* = 8.84, 2.02 Hz, 1H), 7.63 (m, 1H), 7.50 (dd, *J* = 8.21, 4.17 Hz, 1H), 5.15 (q, *J* = 7.07 Hz, 1H), 3.15 (s, 3H), 1.94 (d, *J* = 7.33 Hz, 3H); HPLC purity (method A): RT 6.770, >95%.

(*S*)-6-(1-(6-(3-Fluoro-4-methoxyphenyl)-[1,2,4]triazolo[4,3-*b*]pyridazin-3-yl)ethyl)quinoline (19C). LC-MS *m/z* (M+1)$^+$ 400; ^{1}H NMR (400 MHz, DMSO-*d$_6$*) δ 8.83 (dd, *J* = 4.04, 1.77 Hz, 1H), 8.38(d, *J* = 9.85 Hz, 1H), 8.32(d, *J* = 1.01 Hz, 1H), 7.94−7.99 (m, 2H),

7.90 (d, *J* = 9.85 Hz, 1H), 7.84−7.88 (m, 1H), 7.78−7.85 (m, 2H), 7.50 (dd, *J* = 8.21, 4.17 Hz, 1H), 7.31 (q, 1H), 5.153(q, *J* = 7.33 Hz, 1H), 3.91 (s, 3H), 1.94 (d, *J* = 7.33 Hz, 3H); HPLC purity (method A): RT 6.539, 99%.

(*S*)-6-(1-(6-(4-Methoxy-3-methylphenyl)-[1,2,4]triazolo[4,3-*b*]pyridazin-3-yl)ethyl)quinoline (20C). LC-MS *m/z* (M+1)$^+$ 396; ^{1}H NMR (400 MHz, DMSO-d_6) δ 8.843 (dd, *J* = 4.17, 1.64 Hz, 1H), 8.28−8.37 (m, 2H), 7.93−8.01 (m, 2H), 7.84 (d, *J* = 9.85 Hz, 2 H), 7.79 (dd, *J* = 8.84, 1.77 Hz, 1H), 7.71 (d, *J* = 1.77 Hz, 1H), 7.49 (dd, *J* = 8.34, 4.04 Hz, 1H), 7.05 (d, *J* = 8.59 Hz, 1H), 5.10 (q, *J* = 7.07 Hz, 1H), 2.17 (s, 3H), 1.94 (d, *J* = 7.07 Hz, 3H); HPLC purity (method A): RT 7.165, 96%.

(*S*)-6-(1-(6-(3-Methylphenyl)-[1,2,4]triazolo[4,3-*b*]pyridazin-3-yl)ethyl)quinoline   (21C). LC-MS *m/z* (M+1)$^+$ 366; ^{1}H NMR (400 MHz, DMSO-d_6) δ 8.84 (dd, *J* = 4.04, 1.52 Hz, 1H), 8.38 (d, *J* = 9.85 Hz, 1H), 8.34 (d, *J* = 7.83 Hz, 1H), 8.97−8.01 (m, 2H), 7.87 (d, *J* = 9.85 Hz, 1H), 7.75−7.81 (m, 2H), 7.69 (s, 1H), 7.49 (dd, *J* = 8.34, 4.02 Hz, 1H), 7.40 (t, *J* = 7.71 Hz, 1H), 7.31−7.37 (m, 1H), 5.11 (q, *J* = 7.07 Hz, 1H), 2.34(s, 3H), 1.95 (d, *J* = 7.33 Hz, 3H); HPLC purity (method A): RT 6.985, 98%.

(*S*)-3-(3-(1-(Quinolin-6-yl)ethyl)-[1,2,4]triazolo[4,3-*b*]pyridazin-6-yl)benzonitrile   (15C). LC-MS *m/z* (M+1)$^+$ 377; ^{1}H NMR (400 MHz, DMSO-d_6) δ 8.84 (dd, *J* = 4.24, 1.60 Hz, 1H), 8.42−8.55 (m, 2H), 8.35 (d, *J* = 8.29 Hz, 2H), 7.91−8.12 (m, 4H), 7.71−7.86 (m, 2H), 7.49 (dd, *J* = 8.29, 4.14 Hz, 1H), 5.18 (q, *J* = 7.28 Hz, 1H), 1.96 (d, *J* = 7.16 Hz, 3H); Anal. Calcd for C23H16N6: C, 73.39; H, 4.28; N, 22.33. Found: C, 73.50; H, 4.37; N, 22.39.

(*S*)-4-(3-(1-(Quinolin-6-yl)ethyl)-[1,2,4]triazolo[4,3-*b*]pyridazin-6-yl)benzonitrile   (16C). LC-MS *m/z* (M+1)$^+$ 377; ^{1}H NMR (400 MHz, DMSO-d_6) δ 8.84 (d, *J* = 2.69 Hz, 1H), 8.49 (d, *J* = 9.78 Hz, 1H), 8.35 (d, *J* = 8.44 Hz, 1H), 8.23 (d, *J* = 8.31 Hz, 2H), 8.04 (d, *J* = 8.31 Hz, 2H),

7.95−8.02 (m, 3H), 7.84 (d, *J* = 8.68 Hz, 1H), 7.45−7.53 (m, 1H), 5.11−5.23 (m, *J* = 7.00 Hz, 1H), 1.96 (d, *J* = 7.21 Hz, 3H); HPLC purity (method A): RT 5.717, >95%.

(*S*)-2-(3-(1-(Quinolin-6-yl)ethyl)-[1,2,4]triazolo[4,3-*b*]pyridazin-6-yl)benzonitrile **(22C)**. LC-MS *m/z* (M+1)$^+$ 377; ^{1}H NMR (400 MHz, DMSO-d_6) δ 8.84 (dd, *J* = 1.77, 4.04 Hz, 1H), 8.56 (d, *J* = 9.60 Hz, 1H), 8.30 (d, *J* = 7.58 Hz, 1H), 8.10 (dd, *J* = 1.01, 7.58 Hz, 1H), 7.97 (dd, *J* = 2.78, 5.31 Hz, 3H), 7.73−7.93 (m, 4H), 7.49 (dd, *J* = 4.29, 8.34 Hz, 1H), 5.11−5.19 (m, 1H), 1.92−1.95 (m, 3H); HPLC purity (method B): RT 1.228, >95%.

(*S*)-6-(1-(6-(2,3-Dihydrobenzo[*b*][1,4]dioxin-6-yl)-[1,2,4]triazolo[4,3-*b*]pyridazin-3-yl)ethyl)quinoline (23C). LC-MS *m/z* (M+1)$^+$ 410; ^{1}H NMR (400 MHz, DMSO-d_6) δ 8.83 (dd, *J* = 4.14, 1.70 Hz, 1H), 8.26−8.39 (m, 2H), 7.91−8.01 (m, 2H), 7.75−7.89 (m, 2H), 7.43−7.56 (m, 3H), 6.94−7.05 (m, 1H), 5.11 (q, *J* = 7.16 Hz, 1H), 4.30 (s, 4H), 1.93 (d, *J* = 7.35 Hz, 3H); HPLC purity (method A): RT 6.347, >95%.

(*S*)-*N*-Methyl-4-(3-(1-(quinolin-6-yl)ethyl)-[1,2,4]triazolo[4,3-*b*]pyridazin-6-yl)benzamide (24C). LC-MS *m/z* (M+1)$^+$ 430; ^{1}H NMR (400 MHz, DMSO-d_6) δ 8.83 (dd, *J* = 4.04, 1.52 Hz, 1H), 8.58 (d, *J* = 4.55 Hz, 1H), 8.43 (d, *J* = 9.85 Hz, 1H), 8.35 (d, *J* = 8.08 Hz, 1H), 8.08 (d, *J* = 8.34 Hz, 2H), 7.91−8.02 (m, 5H), 7.82 (dd, *J* = 8.84, 1.77 Hz, 1H), 7.49 (dd, *J* = 8.34, 4.29 Hz, 1H), 5.15 (q, *J* = 7.33Hz, 1H), 2.80 (d, *J* = 4.55 Hz, 3H), 1.95 (d, *J* = 7.33 Hz, 3H); HPLC purity (method A): RT 4.857, 98.5%.

(*S*)-6-(1-(6-(4-Ethanesulfonylphenyl)-[1,2,4]triazolo[4,3-*b*]pyridazin-3-yl)ethyl)quinoline (25C). LC-MS *m/z* (M+1)$^+$ 445; ^{1}H NMR (400 MHz, DMSO-d_6) δ 8.83 (dd, *J* = 4.04, 1.77 Hz, 1H), 8.49 (d, *J* = 9.60 Hz, 1H), 8.37 (dd, *J* = 8.46, 1.14 Hz, 1H), 8.27 (d, *J* = 8.84 Hz, 2H), 8.04 (d, *J* = 8.59 Hz, 2H), 7.95−8.01 (m, 3H), 7.83 (dd, *J* = 8.59, 2.02 Hz, 1H), 7.49 (dd, *J* = 8.34,

4.04 Hz, 1H), 5.15 (q, J = 7.33 Hz, 1H), 3.37 (q, J = 7.33 Hz, 2H), 1.95 (d, J = 7.33 Hz, 3H), 1.11 (t, J = 7.33 Hz, 3H); HPLC purity (method A): RT 5.280, >95%.

(*S*)-6-(1-(6-(4-Methanesulfonylphenyl)-[1,2,4]triazolo[4,3-*b*]pyridazin-3-yl)ethyl)quinoline (26C). LC-MS *m/z* (M+1)$^+$ 430; ^{1}H NMR (400 MHz, DMSO-d_6) δ 8.83 (dd, J = 4.17, 1.64 Hz, 1H), 8.49 (d, J = 9.60 Hz, 1H), 8.36(dd, J = 8.21 Hz, 1.39 Hz, 1H), 8.26 (d, J = 8.59 Hz, 2H), 8.08 (d, J = 8.59 Hz, 2H), 7.96−8.01 (m, 3H), 7.83 (dd, J = 8.57, 2.02 Hz, 1H), 7.49 (dd, J = 8.34, 4.29 Hz, 1H), 5.15 (q, J = 7.33 Hz, 1H), 3.28 (s, 3H), 1.95 (d, J = 7.33 Hz, 3H); HPLC purity (method A): RT 4.857, 98.5%.

(*S*)-*N,N*-Dimethyl-5-(3-(1-(quinolin-6-yl)ethyl)-[1,2,4]triazolo[4,3-*b*]pyridazin-6-yl)pyridin-2-amine (27C). LC-MS *m/z* (M+1)$^+$ 396; ^{1}H NMR (400 MHz, DMSO-d_6) δ 8.73−8.88 (m, 2H), 8.26−8.39 (m, 2H), 8.11 (dd, J = 9.04, 2.45 Hz, 1H), 7.93−8.03 (m, 2H), 7.77−7.90 (m, 2H) 7.49 (dd, J = 8.29, 4.14 Hz, 1H), 6.76 (d, J = 9.23 Hz, 1H), 5.04−5.17 (m, J = 7.35 Hz, 1H), 3.11 (s, 6H), 1.93 (d, J = 7.35 Hz, 3H); HPLC purity (method A): RT 6.007, >99%.

(*S*)-6-(1-(6-(1-Methyl-1*H*-pyrazol-4-yl)-[1,2,4]triazolo[4,3-*b*]pyridazin-3-yl)ethyl)quinoline (8). LC-MS *m/z* (M+1)$^+$ 356; ^{1}H NMR (400 MHz, DMSO-d_6) δ 8.83 (d, J = 2.78 Hz, 1H), 8.46 (s, 1H), 8.35 (d, J = 8.08 Hz, 1H), 8.30 (d, J = 9.60 Hz, 1H), 8.08 (s, 1H), 8.00 (s, 1H), 7.96 (d, J = 8.84 Hz, 1H), 7.83 (d, J = 8.59 Hz, 1H), 7.62 (d, J = 9.85 Hz, 1H), 7.49 (dd, J = 8.34, 4.29 Hz, 1H), 5.04 (q, J = 6.91 Hz, 1H), 3.90 (s, 3H), 1.92 (d, J = 7.33 Hz, 3 H); HPLC purity (method A): RT 4.687, >95%.

(*S*)-6-(1-(6-(1-Methyl-1*H*-pyrazol-4-yl)-1H-[1,2,3]triazolo[4,5-*b*]pyrazin-1-yl)ethyl)quinoline (8D). LC-MS *m/z* 357 (M+H)$^+$; ^{1}H NMR (300 MHz, DMSO-d_6) δ 9.18 (s, 1H), 8.89 (d, J = 4.14 Hz, 1H), 8.62 (s, 1H), 8.40 (d, J = 7.91 Hz, 1H), 8.28 (s, 1H), 7.96−8.11

(m, 2H), 7.84−7.93 (m, 1H), 7.53 (dd, *J* = 4.14, 8.29 Hz, 1H), 6.52−6.63 (m, *J* = 7.30 Hz, 1H),

3.94 (s, 3H), 2.25 (d, *J* = 7.16 Hz, 3H); HPLC purity (method A): RT 11.213, >99%.

(*S*)-2-(4-(1-(1-(Quinolin-6-yl)ethyl)-1H-[1,2,3]triazolo[4,5-*b*]pyrazin-6-yl)-1*H*-pyrazol-1-

yl)ethanol (9D). LCMS *m/z* 387 (M+H)$^+$; ^{1}H NMR (300 MHz, DMSO-*d*$_6$) δ 9.20 (s, 1H), 8.89

(dd, *J* = 1.51, 4.14 Hz, 1H), 8.62 (s, 1H), 8.39 (d, *J* = 7.54 Hz, 1H), 8.30 (s, 1H), 8.08 (s, 1H),

8.02 (d, *J* = 8.85 Hz, 1H), 7.83−7.92 (m, 1H), 7.53 (dd, *J* = 4.24, 8.19 Hz, 1H), 6.53−6.67 (m, *J*

= 7.20 Hz, 1H), 4.98 (br. s., 1H), 4.24 (t, *J* = 5.46 Hz, 2H), 3.78 (d, *J* = 4.71 Hz, 2H), 2.24 (d, *J* =

7.16 Hz, 3H); HPLC purity (method A): RT 10.960, >95%. Anal. Calcd. for C$_{20}$H$_{18}$N$_8$O·0.78

H$_2$O: C, 59.99; H, 4.92; N, 27.98. Found: C, 60.07; H, 4.63; N, 27.78.

3-((1*H*-pyrrolo[2,3-b]pyridin-3-yl)methyl)-6-(1-methyl-1*H*-pyrazol-4-yl)-

[1,2,4]triazolo[4,3-*b*]pyridazine (8E). LC-MS *m/z* 331 (M+H)$^+$; ^{1}H NMR (400 MHz, DMSO-

d$_6$) δ 11.50 (d, *J* = 1.01 Hz, 1H), 8.56 (s, 1H), 8.27−8.33 (m, 1H), 8.15−8.22 (m, 2 H), 8.04 (d, *J*

= 6.57 Hz, 1H), 7.66 (d, *J* = 9.85 Hz, 1H), 7.53 (d, *J* = 2.53 Hz, 1H), 7.03 (dd, *J*= 7.83,4.80 Hz,

1H), 4.60 (s, 2H), 3.94 (s, 3H); HPLC purity (method A): RT 4.080, >97%.

(*S*)-3-(1-(1*H*-pyrrolo[2,3-b]pyridin-3-yl)ethyl)-6-(1-methyl-1*H*-pyrazol-4-yl)-

[1,2,4]triazolo[4,3-*b*]pyridazine (8F). LC-MS *m/z* 345 (M+H)$^+$; ^{1}H NMR (400 MHz, DMSO-

d$_6$) δ 11.47 (s, 1H), 8.50 (s, 1H), 8.27 (d, *J* = 9.61 Hz, 1H), 8.08−8.15 (m, 2H), 7.92−8.00 (m,

1H), 7.61 (d, *J* = 9.80 Hz, 1H), 7.54 (s, 1H), 6.97 (dd, *J* = 7.72, 4.90 Hz, 1H), 5.00−5.14 (m, *J* =

7.35 Hz, 1H), 3.92 (s, 3H), 1.91 (d, *J* = 7.35 Hz, 3H); HPLC purity (method A): RT 4.557,

>95%.

(*S*)-4-(3-(1-(1*H*-pyrrolo[2,3-b]pyridin-3-yl)ethyl)-[1,2,4]triazolo[4,3-*b*]pyridazin-6-

yl)benzonitrile (16F). LC-MS *m/z* 366 (M+H)$^+$; ^{1}H NMR (400 MHz, DMSO-*d*$_6$) δ 11.54 (s,

1H), 8.47 (d, *J* = 9.61 Hz, 1H), 8.25−8.32 (m, 2H), 8.16 (dd, *J* = 4.71, 1.51 Hz, 1H), 8.03−8.09

(m, 2H), 7.95−8.01 (m, 2H), 7.51 (d, J = 2.26 Hz, 1H), 7.01 (dd, J = 7.91, 4.71 Hz, 1H), 5.14

−5.24 (m, J = 7.16 Hz, 1H), 1.91−1.99 (d, J = 7.35, 3 H); HPLC purity (method A): RT 5.486,

>95%.

3-(Quinolin-6-ylmethyl)-[1,2,4]triazolo[4,3-*b*]pyridazin-6-amine (17A). To a solution of

38A (100 mg, 0.338 mmol) in NH_4OH (3 mL, 0.11 M, 28%) was heated in a microwave at 100

°C for 1 hour.   After evaporation, the residue was purified by a preparative HPLC

(acetonitrile/water, with 0.1% HOAc) to obtain **17A** (32 mg, 34% yield). LC-MS *m/z* 276

$(M+H)^+$; ^{1}H NMR (400 MHz, DMSO-d_6) δ 8.85 (dd, J = 4.29, 1.77 Hz, 1H), 8.29 (d, J = 7.33

Hz, 1H), 7.94 (t, J = 8.84 Hz, 2H), 7.78 (s, 1 H), 7.71 (dd, J = 8.84, 2.02 Hz, 1H), 7.50 (dd, J =

8.21, 4.17 Hz, 1H), 6.71−6.84 (m, 3H), 4.52 (s, 2H); HPLC purity (method A): RT 2.564, >95%.

General Procedure B for *N*-replacement reaction.

(S)-3-(1-(1*H*-pyrrolo[2,3-*b*]pyridin-3-yl)ethyl)-*N*-isopropyl-[1,2,4]triazolo[4,3-

***b*]pyridazin-6-amine (28F)**. In a microwave vial was added **38F** (50 mgs, 0.17 mmol), nBuOH

(1 mL), and isopropylamine (1 mL). The reaction was irradiated at 120 °C for 1 hour. LCMS

showed 80% conversion.   Isopropylamine (0.5 mL) was added and irradiated again for 30

minutes at 120 °C. This was repeated three times for full conversion. The reaction was

concentrated and purified by preparatory HPLC eluting with 10-30% acetonitrile/water having

0.1% HOAc to give **28F** as a white amorphous solid (30 mg, 56% yield) after lyophilization.

LC-MS *m/z* $(M+H)^+$ 322; ^{1}H NMR (400 MHz, DMSO-d_6) δ 11.44 (s, 1H), 8.13 (dd, J = 4.71,

1.51 Hz, 1H), 7.85 (dd, J = 7.82, 1.22 Hz, 1H), 7.80 (d, J = 9.98 Hz, 1H), 7.36 (d, J = 2.26 Hz,

1H), 7.13 (d, J = 6.97 Hz, 1H), 6.95 (dd, J = 7.91, 4.71 Hz, 1H), 6.66 (d, J = 9.98 Hz, 1H), 4.85

(q, J = 7.16 Hz, 1H), 3.74−3.91 (m, 1H), 1.84 (d, J = 7.35 Hz, 3H), 1.17 (d, J = 6.40 Hz, 3H),

1.09 (d, J = 6.40 Hz, 3H); HPLC purity (method A): RT 5.601, >99%.

General procedure B was followed for **18A**, **28C** and **29F**.

N,N-Dimethyl-3-(quinolin-6-ylmethyl)-[1,2,4]triazolo[4,3-b]pyridazin-6-amine (**18A**).

LC-MS m/z 305 (M+H)$^+$; ^{1}H NMR (400 MHz, DMSO-d_6) δ 8.85 (dd, J = 4.28, 1.76 Hz, 1H),

8.28−8.37 (m, 1H), 8.00 (d, J = 10.07 Hz, 1H), 7.87−7.97 (m, 2H), 7.76 (dd, J = 8.81, 2.01 Hz,

1H), 7.50 (dd, J = 8.31, 4.28 Hz, 1H), 7.21 (d, J = 10.32 Hz, 1H), 4.57 (s, 2 H), 3.07 (s, 6 H);

HPLC purity (method A): RT 4.691, 96.3%.

(S)-N-Isopropyl-3-(1-(quinolin-6-yl)ethyl)-[1,2,4]triazolo[4,3-b]pyridazin-6-amine (**28C**).

LC-MS m/z 333 (M+H)$^+$; ^{1}H NMR (400 MHz, DMSO-d_6) δ 8.78−8.86 (m, 1H), 8.30 (d, J = 8.34

Hz, 1H), 7.93 (d, J = 8.84 Hz, 1H), 7.87 (s, 1H), 7.82 (d, J = 9.85 Hz, 1H), 7.70 (d, J = 8.59 Hz,

1H), 7.48 (dd, J = 4.29, 8.34 Hz, 1H), 7.12 (d, J = 6.82 Hz, 1H), 6.65 (d, J = 9.85 Hz, 1H), 4.80

(d, J = 7.33 Hz, 1H), 3.76 (d, J = 6.57 Hz, 1H), 1.85 (d, J = 7.33 Hz, 3H), 1.15 (d, J = 6.57 Hz,

3H), 0.93 (d, J = 6.32 Hz, 3H); HPLC purity (method A): RT 5.947, >99%.

(S)-3-(1-(1H-Pyrrolo[2,3-b]pyridin-3-yl)ethyl)-N-ethyl-[1,2,4]triazolo[4,3-b]pyridazin-6-amine (29F). LC-MS m/z 308 (M+H)$^+$; ^{1}H NMR (400 MHz, DMSO-d_6) δ 11.44 (s, 1H), 8.14

(dd, J = 4.71, 1.51 Hz, 1H), 7.88 (dd, J = 7.91, 1.13 Hz, 1H), 7.81 (d, J = 9.80 Hz, 1H), 7.38 (d, J

= 2.26 Hz, 1H), 7.27 (t, J = 5.18 Hz, 1H), 6.96 (dd, J = 7.82, 4.62 Hz, 1H), 6.68 (d, J = 9.80 Hz,

1H), 4.79−4.93 (m, J = 7.35 Hz, 1H), 3.13−3.26 (m, 2H), 1.84 (d, J = 7.16 Hz, 3H), 1.13 (t, J =

7.16 Hz, 3H); HPLC purity (method A): RT 5.080, >95%.

Biochemical kinase assays. c-Met enzyme inhibition was measured by continuous coupled

spectrophotometric assay as previously described.[28] The assay monitored ATP consumption

coupled to oxidation of NADH (measured at 340 nm) while regenerating ATP in the presence of

phosphoenol pyruvate (PEP) and coupling enzymes, pyruvate kinase (PK), and lactic

dehydrogenase (LDH). Assays reactions contained 0.30 mM ATP (4xKm), 0.5 mM Met2

peptide (Ac-ARDMYDKEYYSVHNK), 20 mM $MgCl_2$, 1 mM PEP, 330 µM NADH, 2 mM DTT, 15 units/mL LDH, 15 units/mL PK, test compound (1% DMSO final) in 100 mM HEPES, pH 7.5, 37°C, and the reactions were initiated by adding 50 nM c-Met N-terminal His6-tagged recombinant human enzyme, aa residues 974-1390 (Millipore Corp./Upstate Ltd., Billerica, MA). The inhibitors were shown to be ATP-competitive from kinetic and crystallographic studies, and the dose-response data were fit to the equation for competitive inhibition by the method of nonlinear least-squares (GraphPad Prism, GraphPad Software, San Diego, CA).

Cellular kinase phosphorylation ELISA assays.[27] All experiments were done under standard conditions (37 °C and 5% CO_2). IC_{50} values were calculated by concentration-response curve fitting using a Microsoft Excel–based four-parameter method. Cells were seeded in 96-well plates in media supplemented with 10% fetal bovine serum (FBS) and transferred to serum-free media [with 0.04% bovine serum albumin (BSA)] after 24 h. In experiments investigating ligand-dependent RTK phosphorylation, corresponding growth factors were added for up to 20 min. After incubation of cells with an inhibitor for 1 h and/or appropriate ligands for the designated times, cells were washed once with HBSS supplemented with 1 mmol/L Na_3VO_4, and protein lysates were generated from cells. Subsequently, phosphorylation of selected protein kinases was assessed by a sandwich ELISA method using specific capture antibodies used to coat 96-well plates and a detection antibody specific for phosphorylated tyrosine residues. Antibody-coated plates were (a) incubated in the presence of protein lysates at 4 °C overnight; (b) washed seven times in 1% Tween 20 in PBS; (c) incubated in a horseradish peroxidase–conjugated anti–total-phosphotyrosine (PY-20) antibody (1:500) for 30 min; (d) washed seven times again; (e) incubated in 3,3,5,5-tetramethylbenzidine peroxidase substrate (Bio-Rad) to initiate a colorimetric reaction that was stopped by adding 0.09 N H_2SO_4; and (f) measured for

absorbance in 450 nm using a spectrophotometer.   A549 cell line was used for c-Met cellular

kinase phosphorylation ELISA assay.

In vivo **Subcutaneous xenograft models in athymic mice**.[27] Female nu/nu mice were

obtained from Charles River. Animals were maintained under clean room conditions in sterile

filter top cages with Alpha-Dri bedding and housed on high-efficiency particulate air (HEPA)-

filtered ventilated racks. Animals received sterile rodent chow and water ad libitum. All of the

procedures were conducted in accordance with the Institute for Laboratory Animal Research

Guide for the Care and Use of Laboratory Animals and with Pfizer Animal Care and Use

Committee guidelines. Tumor cells were implanted subcutaneously into the right flank region of

each mouse and allowed to grow to the designated size. The athymic mice bearing established

tumors were administered **8** by oral gavage in 0.5% methylcellulose suspension or 0.5%

methylcellulose solution for the control group. Tumor volume was measured using electronic

digital calipers. Percent (%) inhibition values were calculated as: $100 \times \{1 - [(\text{treated}_{\text{final day}} - \text{treated}_{\text{day 1}})/(\text{control}_{\text{final day}} - \text{control}_{\text{day 1}})]\}$. Tumor volumes were analyzed using one-way

ANOVA. At the end of study, mice were humanely euthanized and tumors were resected.

Proteins were extracted from the tumor samples and protein concentrations were determined

using a BSA assay (Pierce). The level of proteins of interest in the tumor sample was determined

using a capture ELISA method or immunoblotting.

Human microsomal stability studies. Compounds (1 μM) were incubated at 37 °C for

30 min in a final volume of 200 μL of 100 mM potassium phosphate buffer (pH 7.4) containing

pooled human liver microsomes (0.8 mg/mL protein) and 2 mM NADPH.   Reactions were

initiated with the addition of NADPH following a 10-min pre-incubation.   Aliquots of incubation

samples were protein precipitated with cold methanol containing 0.1 μM buspirone (internal

standard) and centrifuged, and supernatants were analyzed by LC-MS/MS. All incubations were performed in triplicate and % remaining of parent drug at the end of incubation was determined by LC-MS/MS peak area ratio.

Cocrystal structures. c-Met cocrystals were obtained at 13 ˚C by the hanging drop vapor diffusion method by mixing 1.2 µL of protein solution (containing 7-13 mg/mL c-Met KD (residues 1051-1348) with a 5 fold molar excess of selected c-Met inhibitor) with 1.2µL of solution containing (0.05 M citrate-phosphate pH 4.6, 0-0.275 M NaCl, and 21% polyethylene glycol MW=3350). Details of the crystal structure determinations can be accessed from the PDB database.

ASSOCIATED CONTENT

Supporting Information.

Figure S1. Metabolite profile of **8F** in human liver microsomes.

Table S1. Profiles of **8** and **9**.

This material is available free of charge via the Internet at http://pubs.acs.org.

AUTHOR INFORMATION

Corresponding Author

*Phone: 858-638-6333. E-mail: jean.cui@pfizer.com

NOTES

The authors declare no competing financial interest.

ACCESSION CODES

PDB accession codes are unphosphorylated c-Met kinase domain with **7** (3zbx), **8** (3zc5), **9** (3zxz), and **28F** (3zcl).

ABBREVIATIONS

A-loop, activation loop; BCR-ABL, breakpoint cluster region-abelson; BZD, benzodiazepine; CDI, 1,1'-carbonyldiimidazole; DIPEA, diisopropylethylamine; EDC, 1-ethyl-3-(3-dimethylaminopropyl)carbodiimide; GABA A, gamma-aminobutyric acid A receptor; GSH, glutathione; HATU, *N*-[(dimethylamino)-1*H*-1,2,3-triazolo-[4,5-b]pyridin-1-ylmethylene]-*N*-methylmethanaminium hexafluorophosphate *N*-oxide; HGF, hepatocyte growth factor; HGFR, hepatocyte growth factor receptor; HLM, human liver microsomes; KD, kinase domain; LipE, lipophilic efficiency; NCE, new chemical entity; NSCLC, non-small cell lung cancer; Pd(dppf)Cl$_2$, [1,1′-bis(diphenylphosphino)ferrocene] dichloropalladium(II); QD, once daily; R&D, research and development; RTK, receptor tyrosine kinase; SF, scatter factor; SFC, supercritical fluid chromatography; TGI, tumor growth inhibition; VHL, von Hippel-Lindau.

REFERENCES

(1) Boccaccio, C.; Comoglio, P. M. Invasive growth: a Met-driven generic programme for cancer and stem cells. *Nat. Rev. Cancer* **2006**, *6*, 637−645.

(2) Knudsen, B. S., Vande Woude, G. Showering c-MET-dependent cancers with drugs. *Curr. Opin. Genet. Dev.* **2008**, *18*, 87−96.

(3) Ma, P. C.; Tretiakova, M. S.; MacKinnon, A. C.; Ramnath, N.; Johnson, C.; Dietrich, S.; Seiwert, T.; Christensen, J. G.; Jagadeeswaran, R.; Krausz, T.; Vokes, E. E.; Husain, A. N.; Salgia, R. Expression and mutational analysis of MET in human solid cancers. *Genes Chromosomes Cancer* **2008**, *47*, 1025–1037

(4) Engelman, J. A.; Zejnullahu, K.; Mitsudomi, T.; Song, Y.; Hyland, C.; Park, J. O.; Lindeman, N.; Gale, C. M.; Zhao, X.; Christensen, J.; Kosaka, T.; Holmes, A. J.; Rogers, A. M.; Cappuzzo, F.; Mok, T.; Lee, C.; Johnson, B. E.; Cantley, L. C.; Jänne, P. A. MET amplication leads to Gefitinib resistance in lung cancer by activating ERBB signaling. *Science* **2007**, *316*, 1039–1043.

(5) Wilson, T. R.; Fridlyand, J.; Yan, Y.; Penuel, E.; Burton, L.; Chan, E.; Peng, J.; Lin, E.; Wang, Y.; Sosman, J.; Ribas, A.; Li, J.; Moffat, J.; Sutherlin, D. P.; Koeppen, H.; Merchant, M.; Neve, R.; Settleman, J. Widespread potential for growth-factor-driven resistance to anticancer kinase inhibitors. *Nature* **2012**, *487*, 505–509.

(6) Straussman, R.; Morikawa, T.; Shee, K.; Barzily-Rokni, M.; Qian, Z.R.; Du, J.; Davis, A.; Mongare, M. M.; Gould, J.; Frederick, D. T.; Cooper, Z. A.; Chapman, P. B.; Solit, D. B.; Ribas, A.; Lo, R. S.; Flaherty, K. T.; Ogino, S.; Wargo, J. A.; Golub, T. R. Tumour micro-environment elicits innate resistance to RAF inhibitors through HGF secretion. *Nature* **2012**, *487*, 500–504.

(7) Yap, T. A.; Sandhu, S. K.; Alam, S. M.; de Bono, J. S. HGF/c-MET targeted therapeutics: novel strategies for cancer medicine. *Curr. Drug Targets* **2011**, *12*, 2045−2058.

(8) Tuma, R. S. Novel antibody, rilotumumab (AMG 102) shows activity in metastatic colorectal cancer patients. *Oncology Times* **2011**, *33*, 22–23.

(9) Surati, M.; Patel, P.; Peterson, A.; Salgia, R. Role of MetMAb (OA-5D5) in c-MET active lung malignancies. *Expert Opin. Biol. Ther.* **2011**, *11*, 1655–1662.

(10) Cui, J. J.; Tran-Dubé, M.; Shen, H.; Nambu, M.; Kung, P. P.; Pairish, M.; Jia, L.; Meng, J.; Funk, L.; Botrous, I.; McTigue, M.; Grodsky, N.; Ryan, K.; Padrique, E.; Alton, G.; Timofeevski, S.; Yamazaki, S.; Li, Q.; Zou, H.; Christensen, J.; Mroczkowski, B.; Bender, S.; Kania, R. S.; Edwards, M. P. Structure based drug design of crizotinib (PF-02341066), a potent and selective dual inhibitor of mesenchymal-epithelial transition factor (c-MET) kinase and anaplastic lymphoma kinase (ALK). *J. Med. Chem.* **2011**, *54*, 6342–6363.

(11) Yakes, F. M.; Chen, J.; Tan, J.; Yamaguchi, K.; Shi, Y.; Yu, P.; Qian, F.; Chu, F.; Bentzien, F.; Cancilla, B.; Orf, J.; You, A.; Laird, A. D.; Engst, S.; Lee, L.; Lesch, J.; Chou, Y. C.; Joly, A. H. Cabozantinib (XL184), a novel MET and VEGFR2 inhibitor, simultaneously suppresses metastasis, angiogenesis, and tumor growth. *Mol Cancer Ther.* **2011**,*10*, 2298−2308.

(12) Munshi, N.; Jeay, S.; Li, Y.; Chen, C. R.; France, D. S.; Ashwell, M. A.; Hill, J.; Moussa, M. M.; Leggett, D. S.; Li, C. J. ARQ 197, a novel and selective inhibitor of the human c-Met receptor tyrosine kinase with antitumor activity. *Mol. Cancer Ther.* **2010**, *9*, 1544–1553.

(13) Peters, S.; Adjei, A. A. MET: a promising anticancer therapeutic target. *Nat. Rev. Clin. Oncol.* **2012**, *9*, 314−326.

(14) Spigel, D. R.; Ervin, T. J.; Ramlau, R.; Daniel, D. B.; Goldschmidt, J. H.; Blumenschein, G. R.; Krzakowski, M. J.; Robinet, G.; Clement-Duchene, C.; Barlesi, F.; Govindan, R.; Patel, T.; Orlov, S. V.; Wertheim, M. S.; Zha, J.; Pandita, A.; Yu, W.; Yauch, R. L.;

Patel, P. H.; Peterson, A. C. Final efficacy results from OAM4558g, a randomized phase II study evaluating MetMAb or placebo in combination with erlotinib in advanced NSCLC. Presented at ASCO 2011 Annual Meeting, Chicago, IL, June 3-7, 2011, Abstr. 7505.

(15) Ou, S.-H. I.; Kwak, E. L.; Siwak-Tapp, C.; Dy, J.; Bergethon, K.; Clark, J. W.; Camidge, D. R.; Solomon, B. J.; Maki, R. G.; Bang, Y.-J.; Kim, D.-W.; Christensen, J.; Tan, W.; Wilner, K.D.; Salgia, R.; Iafrate, A. J. Activity of crizotinib (PF02341066), a dual mesenchymal-epithelial transition (MET) and anaplastic lymphoma kinase (ALK) inhibitor, in a non-small cell lung cancer patient with de novo MET amplification. *J. Thorac. Oncol.* **2011**, *6*, 942−946.

(16) Cui, J. J.; McTigue, M.; Nambu, M.; Tran-Dubé, M.; Pairish, M.; Shen, H.; Jia, L.; Cheng, H.; Hoffman, J.; Le, P.; Jalaie, M.; Goetz, G. H.; Ryan, K.; Grodsky, N.; Deng, Y. L.; Parker, M.; Timofeevski, S.; Murray, B. W.; Yamazaki, S.; Aguirre, S.; Li, Q.; Zou, H.; Christensen, J. Discovery of a novel class of exquisitely selective mesenchymal-epithelial transition factor (c-MET) protein kinase inhibitors and identification of the clinical candidate 2-(4-(1-(quinolin-6-ylmethyl)-1*H*-[1,2,3]triazolo[4,5-*b*]pyrazin-6-yl)-1*H*-pyrazol-1-yl)ethanol (PF-04217903) for the treatment of cancer. *J. Med. Chem.* **2012**, *55*, 8091−8109.

(17) Koenig, M.; Cui, J.; Wei, C. C.; Do, S. H.; Zhang, F.-J.; Vojkovsky, T.; Ramphal, J.; Yang, G.; Mattson, M.; Nelson, C.; Tang, P. C. Indolinone hydrazides as c-met inhibitors. PCT Int. Appl. WO2005005378, **2005**.

(18) The first cocrystal structure of an analogue of **2** with c-Met kinase domain proving the unusual binding mode for exquisite c-MET kinase selectivity was obtained by Nikolaus Schiering and Cinzia Cristiani at legacy Pharmacia in **2002** and was not deposited in PDB.

(19) Vojkovsky, T.; Koenig, M.; Zhang, F.-J.; Cui, J. Tetracyclic compounds as c-Met inhibitors. PCT Int. Appl. WO2005004808, **2005**.

(20) Zhang, F.-J.; Vojkovsky, T.; Huang, P.; Liang, C.; Do, S. H.; Koenig, M.; Cui, J. Preparation of triazolotriazines as c-Met modulators for treating cancer. PCT Int. Appl. WO2005010005, **2005**.

(21) Cui, J.; Botrous, I. Arylmethyl triazolo and imidazopyrazines as c-MET inhibitors. PCT Int. Appl. WO2005004607, **2005**.

(22) Buchanan, S. G.; Hendle, J.; Lee, P. S.; Smith, C. R.; Bounaud, P. Y.; Jessen, K. A.; Tang, C. M.; Huser, N. H.; Felce, J. D.; Froning, K. J.; Peterman, M. C.; Aubol, B. E.; Gessert, S. F.; Sauder, J. M.; Schwinn, K. D.; Russell, M.; Rooney, I. A.; Adams, J.; Leon, B. C.; Do, T. H.; Blaney, J. M.; Sprengeler, P. A.; Thompson, D. A.; Smyth, L.; Pelletier, L. A.; Atwell, S.; Holme, K.; Wasserman, S. R.; Emtage, S.; Burley, S. K.; Reich, S. H. SGX523 is an exquisitely selective, ATP-competitive inhibitor of the MET receptor tyrosine kinase with antitumor activity in vivo. *Mol. Cancer Ther.* **2009**, *8*, 3181−3190.

(23) Perera, T.; Lavrijssen, T.; Janssens, B.; Geerts, T.; King, P.; Mevellec, L.; Cummings, M. D.; Lu, T.; Johnson, D.; Page, M. JNJ-38877605: a selective Met kinase inhibitor

inducing regression of Met-driven tumor models. Presented at the 99th AACR Annual Meeting; 2008 Apr 12–16; San Diego (CA): Abstr 4837.

(24) Liu, X.; Wang, Q.; Yang, G.; Marando, C.; Koblish, H. K.; Hall, L. M.; Fridman, J. S.; Behshad, E.; Wynn, R.; Li, Y.; Boer, J.; Diamond, S.; He, C.; Xu, M.; Zhuo, J.; Yao, W.; Newton, R. C.; Scherle, P. A. A novel kinase inhibitor, INCB28060, blocks c-MET-dependent signaling, neoplastic activities, and cross-talk with EGFR and HER-3. *Clin. Cancer Res.* **2011**, *17*, 7127−7138.

(25) Albrecht, B. K.; Harmange, J.-C.; Bauer, D.; Berry, L.; Bode, C.; Boezio, A. A.; Chen, A.; Choquette, D.; Dussault, I.; Fridrich, C.; Hirai, S.; Hoffman, D.; Larrow, J. F.; Kaplan-Lefko, P.; Jasmine Lin, J.; Lohman, J.; Long, A. M.; Moriguchi, J.; O'Connor, A.; Potashman, M. H.; Reese, M.; Rex, K.; Siegmund, A.; Shah, K.; Shimanovich, R.; Springer, S. K.; Teffera, Y.; Yajing Yang, Y.; Zhang, Y.; Bellon, S. F. Discovery and optimization of triazolopyridazines as potent and selective inhibitors of the c-Met kinase. *J. Med. Chem.* **2008**, *51*, 2879–2882.

(26) Schiering, N.; Knapp, S.; Marconi, M.; Flocco, M. M.; Cui, J.; Perego, Rita.; Rusconi, L.; Cristiani, C. Crystal structure of the tyrosine kinase domain of the hepatocyte growth factor receptor c-MET and its complex with the microbial alkaloid K-252a. *Proc. Natl. Acad. Sci. U.S.A* **2003**, *100*, 12654−12659.

(27) Zou, H. Y.; Li, Q.; Lee, J. H.; Arango, M. E.; Burgess, K.; Qiu, M.; Engstrom, L.; Yamazaki, S.; Parker, M.; Timofeevski, S.; Cui, J. J.; McTigue, M.; Los, M. G.; Bender, S.; Smeal, T.; Christensen, J. G. Sensitivity of Selected Human Tumor Models to PF-

04217903, a Novel Selective c-Met Kinase Inhibitor. *Mol. Cancer Ther.* **2012**, *11*, 1036−1047.

(28) Timofeevski, S. L.; McTigue, M. A.; Ryan, K.; Cui, J.; Zou, H. Y.; Zhu, J. X.; Chau, F.; Alton, G.; Karlicek, S.; Christensen, J. G.; Murray, B. W. Enzymatic characterization of c-MET receptor tyrosine kinase oncogenic mutants and kinetic studies with aminopyridine and triazolopyrazine inhibitors. *Biochemistry* **2009**, *48*, 5339−5349.

(29) Omori, K.; Kotera, J. Overview of PDEs and their regulation. *Circ Res.* **2007**, *100*, 309−327.

(30) Aguirre, S. A., Heyen, J. R.; Collette, W. 3rd; Bobrowski, W.; Blasi, E. R. Cardiovascular effects in rats following exposure to a receptor tyrosine kinase inhibitor. *Toxicol. Pathol.* **2010**, *38*, 416−428.

(31) Hu, W.; Hirakawa, B.; Jessen, B.; Lee, M.; Aguirre, S. A. Tyrosine kinase inhibitor-induced myocardial degeneration in rats through off-target phosphodiesterase inhibition. *J. Appl. Toxicol.* **2012**, *32*, 1008−1020.

(32) Gschwind, A., Fischer, O.M., Ullrich, A. (2004) The discovery of receptor tyrosine kinases: targets for cancer therapy. *Nat. Rev. Cancer*, **4** (5), 361−370.

(33) Scannell, J. W.; Blanckley, A.; Boldon, H.; Warrington, B. Diagnosing the decline in pharmaceutical R&D efficiency *Nature Reviews Drug Discovery* **2012**, *11*, 191−200 .

(34) McKim, J. M. Jr. Building a tiered approach to in vitro predictive toxicity screening: a focus on assays with in vivo relevance. *Combinatorial Chemistry & High Throughput Screening* **2010**, *13*, 188−206.

(35) Edwards, M. P.; Price D. A. Role of physicochemical properties and lipophilic ligand efficiency (LipE or LLE) in addressing drug safety risks. *Annual Reports in Medicinal Chemistry* **2010**, *45*, 381−391.

1
2
3
4
5
6
7
8
9
10
11
12
13
14
15
16
17
18
19
20
21
22
23
24
25
26
27
28
29
30
31
32
33
34
35
36
37
38
39
40
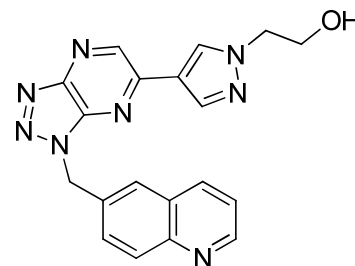41
42
43
44
45
46
47
48
49
50
51
52
53
54
55
56
57
58
59
60

Table of contents graphic
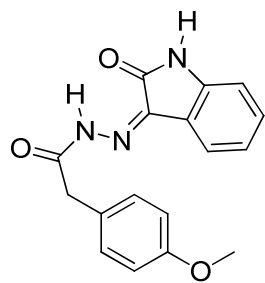
1, HTS Hit
c-MET Ki 0.101 μM
c-MET cell IC$_{50}$ >20 μM
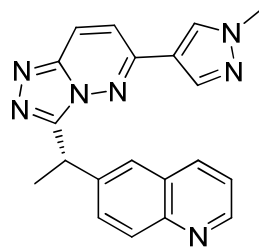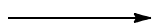
8, **PF-04254644**
c-MET Ki 0.0103 μM
c-MET cell IC$_{50}$ 0.006 μM
Selective over 208 kinases
PDE3B IC$_{50}$ 0.15 μM
Terminated due to cardiotoxicity

9, **PF-04217903**
c-MET Ki 0.004 μM
c-MET cell IC$_{50}$ 0.005 μM
Selective over 208 kinases
PDE3B IC$_{50}$ 5.36 μM
Phase I clinical candidate